Article

Cell

Spliceosomal DEAH-Box ATPases Remodel Pre-mRNA to Activate Alternative Splice Sites

Graphical Abstract

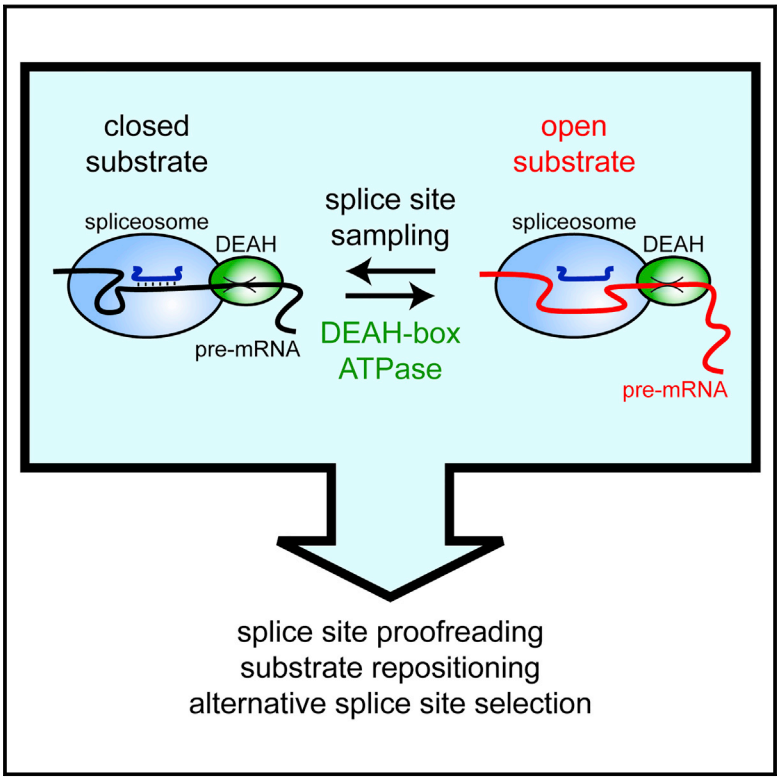

Highlights

- The DEAH-box ATPase Prp16 enables alternative branch site selection
- The DEAH-box ATPase Prp22 promotes alternative 3′ splice site selection
- Prp16 and Prp22 both repress suboptimal sites by disengaging the splice sites
- Prp16 and Prp22 remodel the substrate without translocating through their targets

Authors

Daniel R. Semlow, Mario R. Blanco, Nils G. Walter, Jonathan P. Staley

Correspondence

jstaley@uchicago.edu

In Brief

Two DEAH-box ATPases enable the spliceosome to search for and utilize alternative branch sites and 3′ splice sites by disengaging suboptimal sites from the splicing machinery through a mechanism that suggests action at a distance by RNA pulling.

Semlow et al., 2016, Cell *164*, 985–998
February 25, 2016
http://dx.doi.org/10.1016/j.cell.2016.01.025

CellPress

Article

Cell

Spliceosomal DEAH-Box ATPases Remodel Pre-mRNA to Activate Alternative Splice Sites

Daniel R. Semlow,[1] Mario R. Blanco,[2,3] Nils G. Walter,[3] and Jonathan P. Staley[4,*]
[1]Graduate Program in Cell and Molecular Biology, University of Chicago, 920 East 58th Street, Chicago, IL 60637, USA
[2]Cellular and Molecular Biology, University of Michigan, 930 North University Avenue, Ann Arbor, MI 48109, USA
[3]Single Molecule Analysis Group, Department of Chemistry, University of Michigan, 930 North University Avenue, Ann Arbor, MI 48109, USA
[4]Department of Molecular Genetics and Cell Biology, University of Chicago, 920 East 58th Street, Chicago, IL 60637, USA
*Correspondence: jstaley@uchicago.edu
http://dx.doi.org/10.1016/j.cell.2016.01.025

SUMMARY

During pre-mRNA splicing, a central step in the expression and regulation of eukaryotic genes, the spliceosome selects splice sites for intron excision and exon ligation. In doing so, the spliceosome must distinguish optimal from suboptimal splice sites. At the catalytic stage of splicing, suboptimal splice sites are repressed by the DEAH-box ATPases Prp16 and Prp22. Here, using budding yeast, we show that these ATPases function further by enabling the spliceosome to search for and utilize alternative branch sites and 3′ splice sites. The ATPases facilitate this search by remodeling the splicing substrate to disengage candidate splice sites. Our data support a mechanism involving 3′ to 5′ translocation of the ATPases along substrate RNA and toward a candidate site, but, surprisingly, not across the site. Thus, our data implicate DEAH-box ATPases in acting at a distance by pulling substrate RNA from the catalytic core of the spliceosome.

INTRODUCTION

Pre-mRNA splicing is catalyzed by the spliceosome, a dynamic ribonucleoprotein (RNP) machine comprising over eighty conserved proteins and five small nuclear RNAs (snRNAs) (Wahl et al., 2009). In the first chemical step of splicing, branching, the 2′ hydroxyl of the branch site adenosine (brA) attacks the 5′ splice site phosphate, cleaving the 5′ exon from the intron and forming a lariat intermediate. In the second step, exon ligation, the 3′ hydroxyl of the 5′ exon attacks the 3′ splice site phosphate, joining the exons and excising the lariat intron. Both reactions are enabled by a single catalytic core that is composed of snRNA (Fica et al., 2013; Hang et al., 2015). Within this core, U6 snRNA positions metal ions that participate directly in catalysis (Fica et al., 2013), while the U2 and U6 snRNAs form a base-pairing network that specifies and juxtaposes the reactive splice sites (Hang et al., 2015). However, it remains obscure how the spliceosome accommodates two reactions in a single catalytic core and ensures the fidelity of splice site choice.

The spliceosome faces a formidable challenge in identifying and juxtaposing the appropriate splice sites to ensure faithful gene expression (Semlow and Staley, 2012). The spliceosome must utilize optimal splice sites defined by short nucleotide motifs and discriminate against competing suboptimal splice sites, the utilization of which would corrupt the mRNA. The splice sites are first sampled during spliceosome assembly, which involves the stepwise addition of snRNPs (Wahl et al., 2009). After the 5′ splice site is recognized by the U1 snRNP, the branch site is recognized by the U2 snRNP through base pairing, with bulging of the nucleophilic adenosine, and then the U4/U6.U5 tri-snRNP binds. This assembly pathway and downstream steps require dramatic protein and snRNA rearrangements that depend on eight members of the SF2 superfamily of nucleic acid-dependent ATPases (Figure S1A; Wahl et al., 2009), which function ubiquitously throughout RNA-dependent processes to remodel RNP complexes (Jankowsky, 2011).

Following addition of the U4/U6.U5 tri-snRNP, the assembled but inactive spliceosome is activated in two stages. First, the SF2 ATPase Brr2 disrupts base pairing between U6 and U4 snRNA to permit formation of interactions within U6 and between U6 and U2 snRNA, giving rise to the pre-catalytic spliceosome (Wahl et al., 2009). Then the SF2 ATPase Prp2 promotes a more subtle rearrangement required for branching (Krishnan et al., 2013; Ohrt et al., 2012; Warkocki et al., 2015; Wlodaver and Staley, 2014). Following branching, the SF2 ATPase Prp16 and the Slu7/Prp18 heterodimer act sequentially to reposition the substrate and enable 3′ splice site recognition for exon ligation (James et al., 2002; Ohrt et al., 2013). After exon ligation, the SF2 ATPase Prp22 releases the mRNA from the spliceosome (Company et al., 1991), and the SF2 ATPase Prp43 acts with Brr2 to release the lariat intron and disassemble the spliceosome (Wahl et al., 2009).

At least five SF2 ATPases also promote the fidelity of splicing by discriminating against suboptimal splice sites (Semlow and Staley, 2012). These ATPases likely enable kinetic proofreading by competing with on-pathway events, triggering spliceosomal rearrangements that effectively "reject" suboptimal splice sites.

Despite the importance of spliceosomal SF2 ATPases, the molecular mechanisms by which these ATPase function and their consequences for splice site selection remain largely uncharacterized. Indeed, the functions and mechanisms of only a few SF2 ATPases have been defined in molecular terms (Jankowsky, 2011). Distinct SF2 families appear to perform different

functions and by distinct mechanisms (Ozgur et al., 2015). The spliceosomal SF2 members belong to the DEAD-box family or the DExH-box families, which include the Ski2-like, DEAH-box, and viral NS3/NPH-II families. By directly binding and distorting a duplex, DEAD-box ATPases unwind double-stranded RNA. The DExH-box families are also thought to unwind RNA but by translocating through a duplex, 3′ to 5′ along a single strand of RNA. Indeed, Ski2-like ATPases include a duplex-melting element. However, this element is not conserved in DEAH-box or NS3/NPH-II ATPases (Jankowsky, 2011; Prabu et al., 2015), raising questions about their functions and mechanisms.

At the catalytic stage of splicing, the DEAH-box ATPases Prp16 and Prp22 also contribute to the fidelity of branching and exon ligation, respectively (Semlow and Staley, 2012). In addition to promoting repositioning of an optimal substrate after branching, Prp16 rejects suboptimal branch sites by competing with branching to remodel the spliceosome into an inactive conformation (Burgess and Guthrie, 1993; Koodathingal et al., 2010). By genetics, Prp16 appears to both reject a suboptimal substrate and promote an optimal substrate in a similar manner (Hilliker et al., 2007; Mefford and Staley, 2009; Villa and Guthrie, 2005). However, the mechanism by which Prp16 rejects a suboptimal substrate and promotes an optimal substrate remains unclear.

In addition to promoting mRNA release after exon ligation, Prp22 rejects a suboptimal 3′ splice site by competing with exon ligation to remodel the spliceosome into an inactive conformation (Mayas et al., 2006). Because of these two roles, we proposed that Prp22 effects both activities by translocating upstream from the 3′ exon to disrupt interactions between the spliceosome and the substrate, interactions that differ before and after exon ligation due to the changing connectivity of the substrate (Mayas et al., 2006). Indeed, mRNA release requires that Prp22 interact with the 3′ exon (Schwer, 2008). However, the mechanism by which Prp22 rejects a suboptimal 3′ splice site remains undefined and evidence for translocation before or after exon ligation is lacking.

The rejection of a splice site by Prp16 or Prp22 can be followed by the termination of splicing and discard of the substrate by the spliceosome disassembly factor Prp43 (Koodathingal et al., 2010; Mayas et al., 2010). However, rejection by Prp16 or Prp22 can also be followed by rebinding of the substrate (Koodathingal et al., 2010; Mayas et al., 2006), though the function of this rebinding is unknown.

Here, using budding yeast, we have investigated the function and mechanism of DEAH-box ATPases during the catalytic stage of splicing. Unexpectedly, we discovered that rejection of suboptimal splice sites by the ATPases Prp16 and Prp22 enables the spliceosome to select alternative splice sites. Utilizing single-molecule fluorescence resonance energy transfer (smFRET), we found that these ATPases generally promote splice site rejection and substrate repositioning by disengaging splice sites. Finally, we revealed evidence that these ATPases reject suboptimal substrates and promote optimal substrates by translocating along substrate RNA downstream of the catalytic core, but not necessarily through interactions targeted for disruption. Overall, our results support a model in which these DEAH-box ATPases function by pulling on the RNA substrate to destabilize substrate-spliceosome interactions, thereby enabling the spliceosome to sample alternative interactions with the substrate.

RESULTS

The DEAH-Box ATPase Prp16 Enables Alternative Branch Site Selection

To investigate the mechanism of Prp16-mediated branch site rejection, we designed a splicing substrate that would allow assembly of catalytically active spliceosomes but preclude branching. Specifically, we incorporated deoxyadenosine at the canonical branch site of a *UBC4* pre-mRNA, eliminating the nucleophilic 2′ hydroxyl (d-brA; Figure 1A). Despite our design, in yeast whole-cell extract the d-brA substrate branched (Figure 1B, lanes 1 and 5) using an alternative branch site (see below; c.f. Query et al., 1994). Unexpectedly, depletion of Prp16, which is canonically required only for exon ligation (Figure 1B, lanes 2–4), completely abolished branching of the d-brA substrate, and wild-type, but not ATPase-defective, recombinant (r)Prp16 rescued branching (Figure 1B, lanes 6–8). Thus, the activation of alternative branch sites required Prp16.

To test whether Prp16 was sufficient to activate alternative branch sites, we depleted Prp16 from extract, assembled spliceosomes on the d-brA substrate and isolated the stalled spliceosomes from extract by gradient fractionation. Note that by smFRET, the pre-mRNA adopted a conformation indistinguishable from the catalytically active conformation (see below), implying that spliceosomes stalled solely due to the lack of the 2′ hydroxyl nucleophile. Importantly, wild-type, but not ATPase-defective, rPrp16 chased the isolated spliceosomes through branching; rSlu7/rPrp18 chased the spliceosomes further through exon ligation (Figure 1C). Thus, Prp16 was sufficient to activate alternative branch sites within assembled spliceosomes.

Interestingly, branching of the d-brA substrate yielded distinct lariat intermediates (Figures 1B and 1C) resulting from branching at alternative adenosines 1 and 4 nt upstream of the consensus branchpoint (Figure 1D). Because branching at −4 has not been observed in the context of canonical U2-branch site base pairing (Smith et al., 2009), branching at −4 implies that Prp16 destabilized the branch site-U2 interaction, allowing the splicing substrate to re-align with U2. Indeed, the sequence flanking this alternative branch site is complementary to U2 and bulges the nucleophilic adenosine (Figure 1D), and mutations that eliminate the complementarity precluded formation of the faster-migrating lariat intermediate (Figure S1B). Thus, we infer that in rejecting a branch site, Prp16 triggers unwinding of the U2-branch site interaction and thereby enables the selection of alternative branch sites (see Discussion).

Prp16-Mediated Rejection Antagonizes Juxtaposition of the Branch Site and 5′ Splice Site

While depletion of Prp16 stalls the d-brA substrate before branching, the spliceosome nevertheless juxtaposes the deoxyadenosine branch site with the 5′ splice site (see below), suggesting that Prp16 not only disrupts the U2-branch site interaction but also antagonizes juxtaposition of the branch site with the 5′ splice site. To test the possibility that Prp16

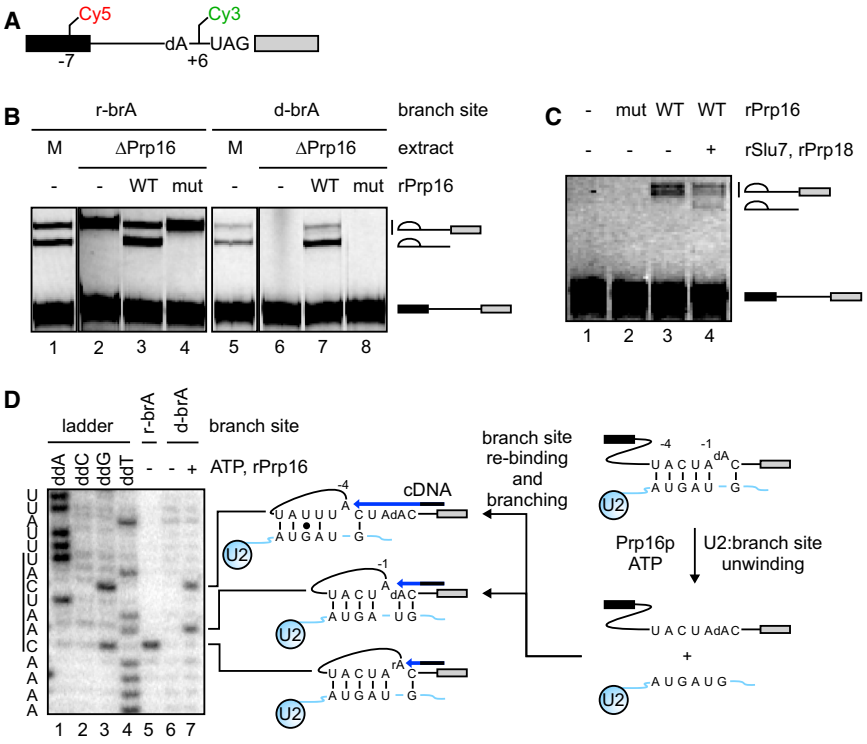

Figure 1. Prp16 Promotes Sampling of Alternative Branch Sites

(A) Schematic of synthetic fluorescently labeled splicing substrate with a deoxyadenosine substitution at the canonical branch site (d-brA).

(B) Splicing of r-brA and d-brA substrates was tested in mock- (M) or Prp16-depleted (ΔPrp16) extract, supplemented with exogenous wild-type (WT) or K379A-mutated (mut) rPrp16.

(C) Isolated, Prp16-depleted spliceosomes assembled on d-brA substrate were incubated with the indicated factors. Splicing was visualized in (B) and (C) via Cy3.

(D) The r-brA and d-brA substrate branchpoints were mapped by extension of a ^{32}P-labeled primer. Stops occur 1 nucleotide (nt) downstream of the branch site, as diagrammed. The inferred activity of Prp16 is modeled in the cartoon.

See also Figure S1.

antagonizes splice site juxtaposition, we monitored splice site proximity by smFRET (Abelson et al., 2010; Blanco et al., 2015; Krishnan et al., 2013), which enables an assessment of substrate conformation in crude preparations with limiting amounts of substrate in multiple conformations. We assembled spliceosomes on *UBC4* splicing substrates labeled with a fluorescent acceptor just upstream of the 5′ splice site and a fluorescent donor just downstream of the branch site (BS labeled; Figure 2A; Table S1; Krishnan et al., 2013). To facilitate the assignment of a FRET state to a specific intermediate, we enriched for distinct intermediates by (1) stalling particular intermediates through inactivation of individual SF2 ATPases (Figure S1A), (2) isolating these intermediates from cell extract by gradient fractionation, and (3) immobilizing these intermediates on slides for total internal reflection fluorescence (TIRF) microscopy through specific affinity tags on individual spliceosomal components (Figure 2A). We then sampled emission trajectories (Figure 2A; Table S2) to generate histograms that describe the frequency with which spliceosomes at a particular intermediate stage occupy a given FRET state.

We first defined reference FRET states by assessing juxtaposition of the branch site and 5′ splice site during spliceosome assembly and activation. The splicing substrate exhibited (1) a zero FRET state in assembled but catalytically inactive spliceosomes (Figure 2B), (2) a low (0.29) FRET state in pre-catalytic spliceosomes (Figure 2C), and (3) a high (0.75) FRET state in spliceosomes stalled at the branching stage (Figure 2D); FRET peaks for a specific intermediate varied with an SD of ±0.04. These FRET states were static (Figure S2A; Table S2), precluding direct analysis of substrate dynamics but still allowing assessment of substrate conformation in distinct spliceosomal subpopulations. Consistent with previous studies, and thereby validating our approach (Blanco et al., 2015; Crawford et al., 2013; Krishnan et al., 2013), these increasing FRET states indicate stepwise juxtaposition of the branching reactants.

To test the consequences of Prp16-mediated rejection on the juxtaposition of the branch site with the 5′ splice site, we utilized a model system for investigating proofreading in vitro (Figure S2B). In this system, spliceosomes stall just before branching due to U6 snRNA phosphorothioate substitutions that compromise the coordination of catalytic metals (Fica et al., 2013); this stalling is due in part to rejection by Prp16 (Koodathingal et al., 2010). Because these substitutions, unlike branch site mutations, permit efficient spliceosome assembly in vitro, we assayed substrate juxtaposition during Prp16-dependent rejection of one such substitution, U80-PS(S_P), in which the *pro*-S_P phosphate oxygen at nucleotide U80 was substituted with sulfur (Koodathingal et al., 2010).

As expected, isolated spliceosomes reconstituted with U6 U80-PS(S_P) and assembled on BS-labeled substrate did not catalyze branching in Mg^{2+} but did in Cd^{2+}, which restored metal binding to U80-PS(S_P) (Figure S2C). U6 U80-PS(S_P) spliceosomes that were stalled before (in Mg^{2+}) and after (in Cd^{2+}) branching both exhibited high FRET states (0.73 and 0.76, respectively; Figures 2F and 2E, respectively, and Figure 2H), indicating that substrate juxtaposition is not appreciably altered by branching. Spliceosomes stalled before branching by the d-brA branch site also exhibited a high FRET state (0.70; Figure S2D). These data imply that spliceosomes containing either the d-brA or U6 U80-PS(S_P) perturbation stall with the reactants poised for chemistry (Figure 1; Koodathingal et al., 2010).

Next, we activated Prp16-dependent rejection by incubating isolated U6 U80-PS(S_P) spliceosomes, stalled in Mg^{2+} before branching, with ATP and then immobilized spliceosomes on slides and washed to remove ATP and unbound splicing factors,

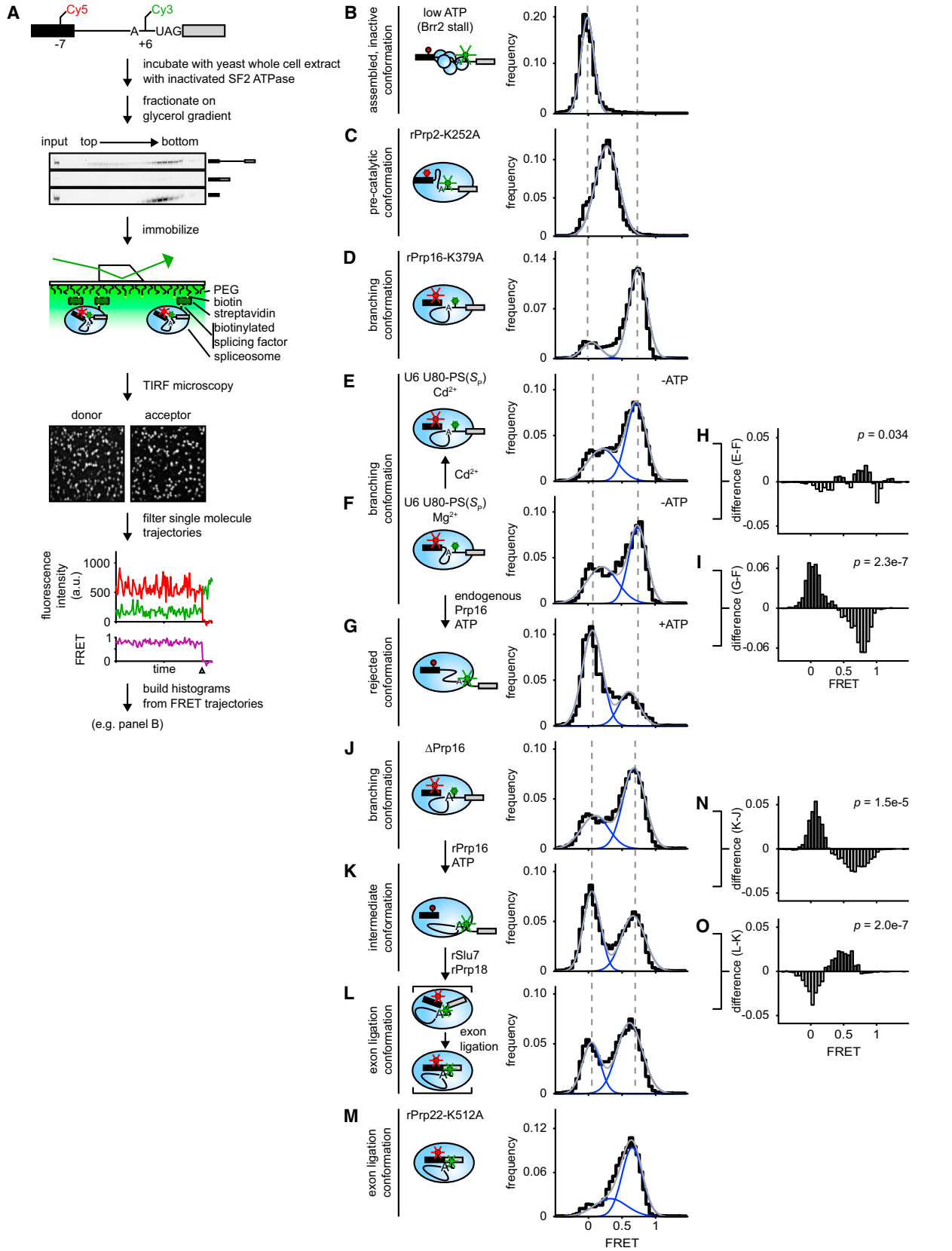

(legend on next page)

quenching the reaction. Strikingly, activation of Prp16-mediated rejection shifted U80-PS(S_P)-stalled spliceosomes from the high FRET state to a near-zero FRET state (0.07; Figures 2G and 2I); this shift was blocked by the ATPase-deficient mutant rPrp16-K379A (Figure S2E). These findings further support a model in which Prp16 rejects a branch site by disrupting the U2-branch-site interaction and, as a consequence, disengaging the branch site from the 5′ splice site.

Prp16 Also Antagonizes Juxtaposition of the Branch Site and 5′ Exon after Branching

To determine the consequences of Prp16 action on the juxtaposition of the 5′ exon with the branch site after branching, we stalled Prp16-depleted spliceosomes just after branching, isolated these spliceosomes by gradient fractionation, added back rPrp16 and ATP (Figure S2F), and then immobilized the spliceosomes for TIRF microscopy, washing away ATP and unbound factors. Strikingly, wild-type, but not mutated, rPrp16 shifted a subpopulation of spliceosomes assembled on BS-labeled substrate from the high FRET state exhibited by the branching conformation (Figure 2J) to a near-zero FRET state indicative of an open substrate conformation (0.07; Figures 2K and 2N; Figure S2G), paralleling the Prp16-dependent formation of a low FRET state before branching (compare Figures 2F and 2G). Thus, after branching, Prp16 appears to function in an ATP-dependent manner to separate the products of the branching reaction, just as it appears to function before branching to separate the reactants. Because genetics have implicated unwinding of the branch site-U2 interaction after branching (Kannan et al., 2013), Prp16 may separate the branching products by disrupting this interaction, just as it does before branching (see Discussion).

To test for evidence that the Prp16-dependent, near-zero FRET state, intermediate conformation is functional, we added rSlu7 and rPrp18 to the spliceosomes activated as above with rPrp16 and ATP, to drive mRNA formation (Figure S2F). Indeed, rSlu7/rPrp18 shifted a subpopulation of spliceosomes from the near-zero FRET state back to a high FRET state (0.63; Figures 2L and 2O), characteristic of the exon ligation conformation (0.67; Figure 2M; Figure S1A), and with an efficiency expected given the degree of mRNA formation (Figure S2F). Note that the high FRET state at exon ligation implies that the branch site is an integral component of the catalytic core at this stage, consistent with the deleterious effects of branch site mutations at exon ligation. Overall, our data support a model in which Prp16 drives separation of the branch site and 5′ exon, thereby allowing Slu7 and Prp18 to establish a proximal configuration of the branch site and 5′ exon in the exon ligation conformation, a configuration that likely accommodates 3′ splice site binding.

Evidence that Prp16 Translocates toward, but Not through, the Branch Site U2-Interaction

Next, we investigated how Prp16 might disrupt the branch site-U2 interaction in antagonizing juxtaposition of splicing reactants before branching and products after branching. Prp16 crosslinks with substrate downstream of the branch site (McPheeters and Muhlenkamp, 2003) and unwinds model RNA duplexes with a 3′ to 5′ polarity (Wang et al., 1998). Thus, we hypothesized that Prp16 translocates 3′ to 5′ along substrate RNA, initiating downstream of the branch site and translocating toward and then across the branch site to disrupt the U2-branch site interaction.

Consequently, to test whether Prp16-mediated rejection requires substrate downstream of the branch site, we assembled and stalled spliceosomes on the d-brA substrate in Prp16-depleted extract, isolated the spliceosomes by gradient fractionation, cleaved the spliceosome-bound substrate downstream of the branch site by oligomer-directed RNase H, and then assayed for chase through branching at alternative branch sites upon addition of ATP and rPrp16 (Figure 3A). Cleavage between +9 and +23 nucleotides, but not between +16 and +33, relative to the canonical branch site blocked the Prp16-dependent chase (Figure 3A, lanes 5 and 7); note that a truncation even closer to an active branch site did not compromise the branching reaction itself (Figure S3A). Thus, substrate downstream of the branch site is required for the Prp16-dependent rejection of the d-brA branch site.

Next, we tested whether the requirement for substrate nucleic acid downstream of the branch site was specific for RNA, because the ATPase activity of Prp16 is stimulated by single-stranded RNA (ssRNA), but not by single-stranded DNA (ssDNA) (Schwer and Guthrie, 1991). The catalytic, RecA-like domains of SF2 ATPases interact with a minimum of 5 nt of RNA (Ozgur et al., 2015), so we substituted substrates with DNA in 8 nt, tiled windows downstream of the branch site (Figure 3B). With the r-brA substrate, DNA substitutions of +6 to +12 through +12 to +19 compromised branching (Figure S3B), precluding a test of whether these substitutions impede Prp16. Still, upstream DNA substitutions at +2 to +9, +3 to +10, and +4 to +11 permitted branching of the r-brA substrate (see below). In striking contrast, with the d-brA substrate the DNA substitutions at +3 to +10

Figure 2. Prp16 Promotes Separation of the 5′ Exon and Branch Site during Both Rejection before Branching and Remodeling after Branching

(A) Workflow for smFRET experiments.

(B–G) Spliceosomal FRET distributions.

(H and I) Difference histograms conveying changes in FRET distribution; difference histograms were generated by subtracting the values for each bin in the indicated panels.

(J–M) Spliceosomal FRET distributions.

(N and O) Difference histograms generated as in (H) and (I).

For (B)–(G) and (J)–(M), spliceosomes were stalled and isolated by gradient fractionation or also chased (E, G, K, and L), as indicated. Histograms (black) were fitted with Gaussian peaks (blue) with the indicated sum (gray; see Table S2 for details). Diagrams describe substrate connectivity and inferred substrate arrangement based on FRET state for the major spliceosomal conformation in each population. p values were determined as described in the Supplemental Experimental Procedures.

See also Figure S2 and Table S2.

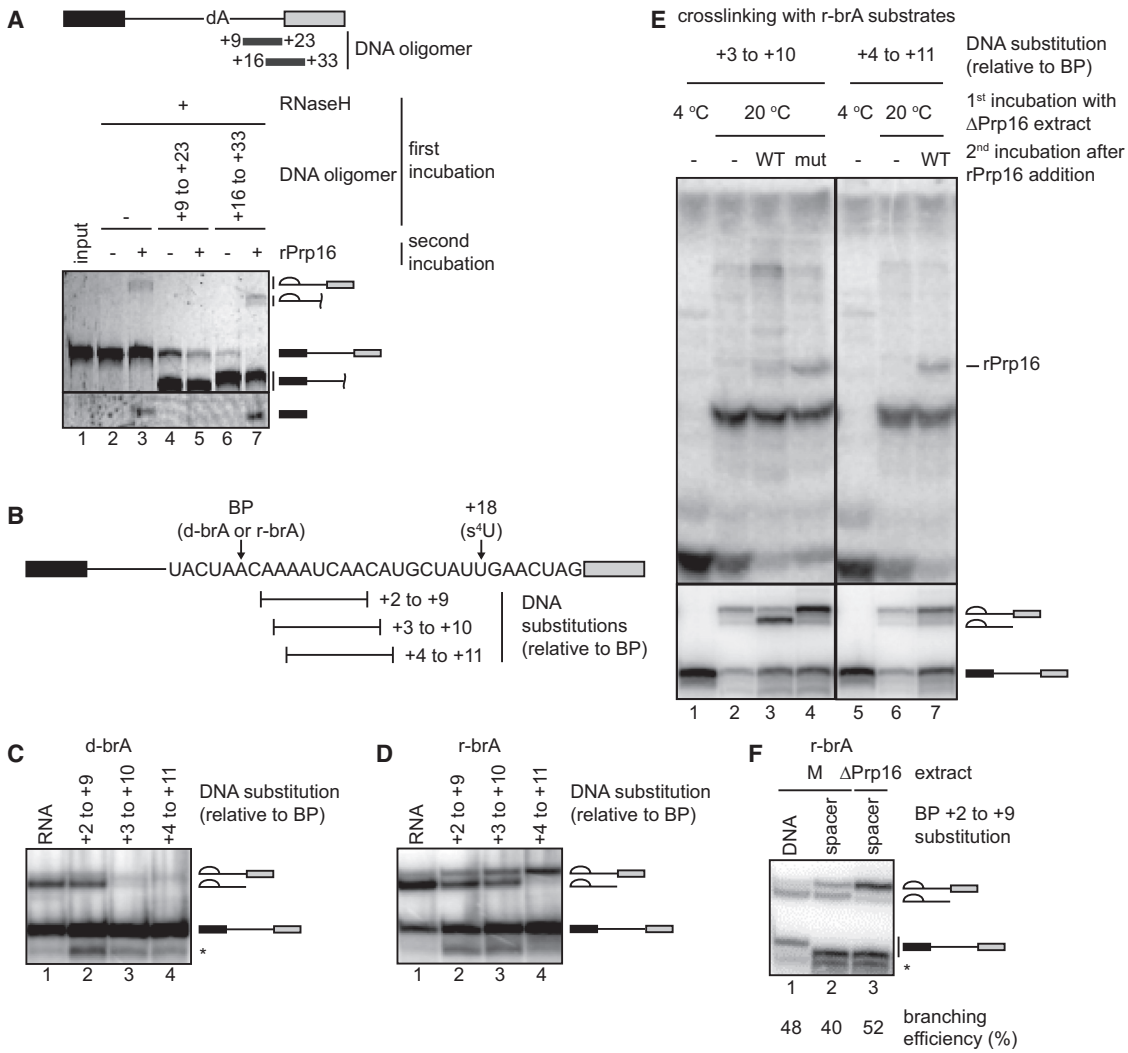

Figure 3. Prp16 Rearranges the Substrate by Translocating toward, but Not through, Interactions with the Spliceosome

(A) The diagram indicates regions of the substrate complementary to DNA oligomers (positions are relative to the branch site) that directed RNaseH cleavage. Pre-mRNA and lariat intermediates were visualized via Cy3. The free 5' exon was visualized via Cy5.

(B) Schematic of substrates with substitutions downstream of the branch site used in (C) to (F).

(C and D) Splicing of d-brA (C) or r-brA (D) substrates with deoxy substitutions at the positions indicated.

(E) The r-brA substrates with the indicated deoxy substitutions and a 4-thio-U modification were incubated and chased as indicated with wild-type (WT) or K379A-mutated (mut) rPrp16 and then crosslinked. Transfer of radiolabel from the substrate to crosslinked protein was analyzed by SDS-PAGE (top); splicing was monitored by PAGE (bottom).

(F) Splicing of an r-brA substrate with carbon spacer substitution at the position indicated. Bands marked with an asterisk in (C), (D), and (F) reflect degradation of the pre-mRNA up to the DNA or spacer substitution.

See also Figure S3.

and +4 to +11 inhibited branching (Figure 3C, lanes 3 and 4). Thus, the activation of alternative branch sites requires both Prp16 and RNA downstream of the branch site, supporting the model in which Prp16 interacts with the substrate downstream of the branch site and translocates upstream. Importantly, however, the DNA substitution at +2 to +9 did not inhibit branching of the d-brA substrate (Figure 3C, lane 2). Similarly, with the r-brA substrate, a DNA substitution at +4 to +11 inhibited exon ligation, but the substitutions at +2 to +9 and +3 to +10 did not (Figure 3D). Thus, unexpectedly, our data suggest a refined model in which Prp16 does translocate 3′ to 5′ toward the branch site, but not through the U2-branch site interaction.

To rule out that DNA substitutions downstream of the branch site simply blocked recruitment of Prp16 to the substrate, we assayed the impact of DNA substitutions on the previously established interaction between Prp16 and substrate 18 nt downstream of the branch site (McPheeters and Muhlenkamp, 2003). We depleted Prp16 from extract, assembled spliceosomes on r-brA substrates substituted with DNA at +3 to +10 or +4 to +11 and the crosslinker 4-thio-U (s^4U) at +18, stalled

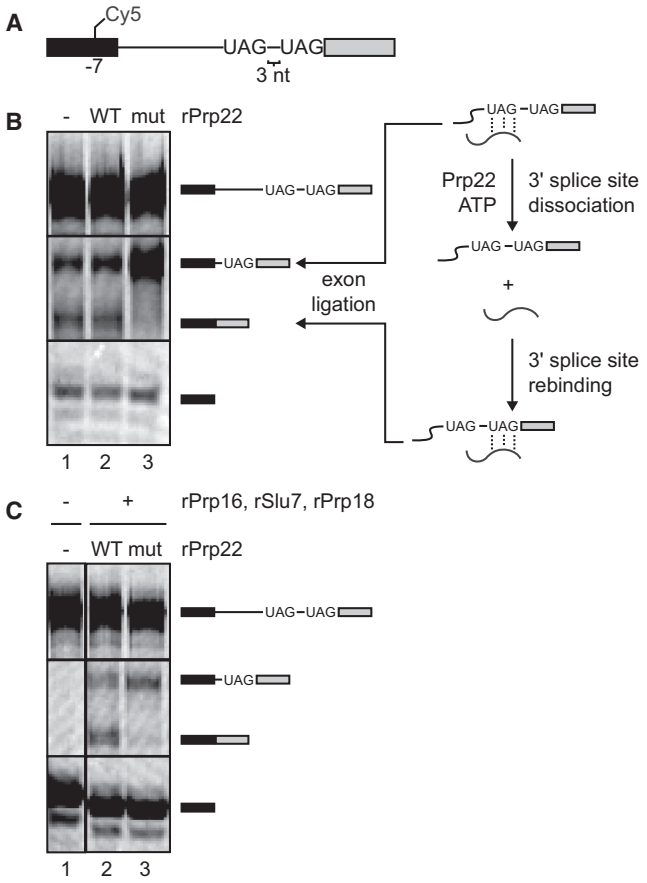

Figure 4. Prp22 Promotes Sampling of Alternative 3′ Splice Sites

(A) Schematic of synthetic, fluorescently labeled splicing substrate with tandem 3′ splice sites.

(B) Splicing of the tandem substrate in extract containing only endogenous Prp22 (–) or also exogenous wild-type (WT) or K512A-mutated (mut) rPrp22. Splicing was visualized via Cy5. The inferred activity of Prp22 is modeled in the cartoon.

(C) Isolated, Prp16-depleted spliceosomes assembled on the tandem substrate were incubated with the indicated factors.

the spliceosomes just after branching, added back rPrp16, and finally photo-activated crosslinking of the substrate with UV. With the permissive +3 to +10 DNA substitution, we observed a crosslink to Prp16 that we confirmed based on (1) migration at the expected molecular weight, (2) a dependence on spliceosome activation (Figures S3C and S3D), (3) a dependence on the addition of rPrp16 (Figure 3E, lanes 2 and 3), and (4) an increase with mutated rPrp16 that correlated with the accumulation of lariat intermediate (Figure 3E, lanes 3 and 4). Importantly, wild-type rPrp16 crosslinked more efficiently to the restrictive +4 to +11 DNA-substituted substrate than to the permissive +3 to +10 DNA-substituted substrate, paralleling the accumulation of the +4 to +11 lariat intermediate (Figure 3E, lane 7). Thus, the +4 to +11 DNA substitution did not block exon ligation by impeding Prp16 recruitment.

Overall, these data support the refined model in which Prp16 translocates toward, but not through, the U2-branch site interaction. Indeed, Prp16 also crosslinks at +11, but not at +6 (McPheeters and Muhlenkamp, 2003). Formally, Prp16 might indirectly disrupt the U2-branch site interaction by displacing a factor that interacts with the substrate downstream of the branch site, but a substitution of +2 to +9 with an equivalent-length carbon spacer, which would destabilize interactions with bound factors, permitted efficient branching (Figure 3F), and the further downstream region of +9 to +23 was accessible to RNaseH-mediated digestion (Figure 3A), providing no evidence for functional or stable binding of factors downstream of the branch site. Further, the carbon spacer did not bypass the requirement for Prp16 (Figure 3F), arguing against a role for Prp16 in displacing a factor bound downstream of the branch site. Thus, we favor the refined model in which Prp16 translocates 3′ to 5′ along the substrate toward, but not through, the branch site. This model implies that Prp16 disrupts the U2-branch site interaction from a distance by moving the RNA substrate relative to the spliceosome, thereby pulling the substrate and applying tension sufficient to disrupt the U2-branch site interaction (see Discussion).

The DEAH-Box ATPase Prp22 Enables Alternative 3′ Splice Site Selection

Given the role for Prp22 in rejecting 3′ splice sites (Mayas et al., 2006), we tested whether Prp22 enables the spliceosome to select alternative 3′ splice sites. In the presence of extract containing only endogenous Prp22 or also exogenous wild-type rPrp22, exon ligation of a substrate with tandem alternative 3′ splice sites occurred at both the upstream and downstream 3′ splice sites (Figures 4A and 4B, lanes 1 and 2). However, in the presence of dominant-negative, ATPase-defective rPrp22-K512A, which blocks rejection of a 3′ splice site (Mayas et al., 2006), exon ligation occurred exclusively at the upstream 3′ splice site (Figure 4B, lane 3). To test the sufficiency of Prp22 and other canonical exon ligation factors in the activation of the downstream 3′ splice site, we isolated, by gradient fractionation, Prp16-depleted spliceosomes stalled just after branching (Figure 4C, lane 1) and then chased the spliceosomes with ATP, rPrp16, rSlu7, and rPrp18, along with wild-type or mutated rPrp22 (Figure 4C, lanes 2 and 3). Again, wild-type rPrp22 permitted splicing at both splice sites, whereas rPrp22-K512A restricted splicing to the upstream 3′ splice site. Thus, use of the downstream 3′ splice site requires the ATP-dependent function of Prp22, implying that recognition of the downstream 3′ splice site requires Prp22-dependent rejection of the upstream 3′ splice site (see Discussion), which is reminiscent of the repression of silent, upstream 3′ splice sites in human splicing extract by hSlu7 (Chua and Reed, 1999), which in budding yeast recruits Prp22. We conclude that Prp22, similar to Prp16, facilitates alternative splice site selection.

Prp22-Mediated Rejection Antagonizes Juxtaposition of the 3′ Splice Site with the 5′ Exon

To test whether Prp22-dependent rejection, like Prp16-dependent rejection, antagonizes juxtaposition of the reactants, we monitored splice site proximity in specific spliceosomal intermediates by smFRET using a substrate labeled with a fluorescent acceptor in the 5′ exon and a fluorescent donor just downstream of the 3′ splice site (3′SS-labeled substrate; Figure 5A; Table S1).

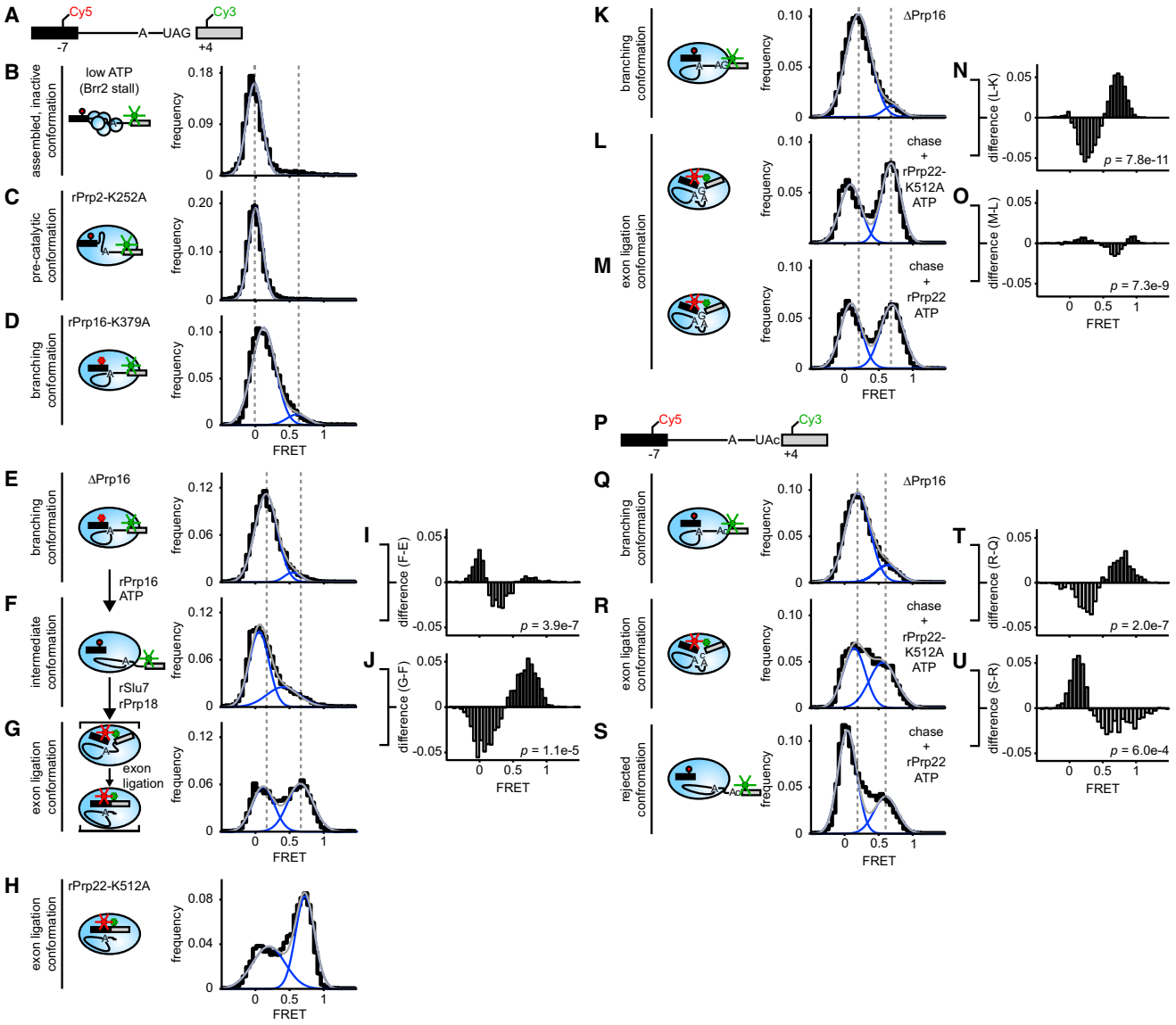

Figure 5. Prp22 Promotes Separation of the 5′ Exon and 3′ Splice Site during Rejection before Exon Ligation

(A) Schematic of fluorescently labeled synthetic splicing substrate with optimal (UAG) 3' splice site.

(B–H) Spliceosomal FRET distributions.

(I and J) Difference histograms conveying changes in FRET distribution; histograms and p values were generated as in Figure 2.

(K–M) Spliceosomal FRET distributions.

(N and O) Difference histograms; histograms and p values were generated as in Figure 2.

(P) Schematic of fluorescently labeled synthetic splicing substrate with suboptimal (UAc) 3' splice site.

(Q–S) Spliceosomal FRET distributions.

(T and U) Difference histograms; histograms and p values were generated as in Figure 2.

For (B)–(H), (K)–(M), and (Q)–(S), spliceosomes were stalled and isolated or also chased (F, G, L, M, R, and S), as indicated. For (L), (M), (R), and (S), Prp16-depleted spliceosomes were chased with rPrp16, rSlu7, and rPrp18 (chase) and wild-type or K512A-mutated rPrp22, as indicated. Histograms were fitted as in Figure 2. See also Figure S4 and Table S2.

This substrate efficiently reported on the juxtaposition of the 5′ exon with the 3′ splice site at the exon ligation stage, as revealed by a high (0.74) FRET signal (Figures 5H and S1A; Abelson et al., 2010).

We first determined the timing for juxtaposing the 3′ splice site with the 5′ exon, as above (Figure 2). FRET states were again static (Figure S4A; Table S2). The assembled but inactive spliceosome conformation, the pre-catalytic conformation, and the branching conformation exhibited near-zero and low FRET states (Figures 5B–5D), indicating that the 3′ splice site does not juxtapose (Figure 2) with the 5′ splice site before or during branching. Spliceosomes stalled after branching by depletion

of Prp16 and then chased with rPrp16 into the intermediate conformation remained in a low FRET state (Figures 5E, 5F, 5I, and S4B), but spliceosomes driven further into the exon ligation conformation, by the addition of rSlu7 and rPrp18, exhibited a high (0.67) FRET state (Figures 5G, 5J, and S4B). Thus, Prp16 first separates the 5′ exon from the branch site (Figure 2), and then Slu7 and Prp18 juxtapose the 5′ exon with the 3′ splice site, as well as the branch site (Figures 2 and 5).

Next, we assayed the impact of Prp22-mediated rejection on the juxtaposition of the 5′ exon with a suboptimal 3′ splice site (Figure 5P) by assembling spliceosomes on 3′SS-labeled substrate in extracts depleted of Prp16, isolating stalled spliceosomes by gradient fractionation (Figures 5K and 5Q) and then chasing with rPrp16, rSlu7, and rPrp18 and either wild-type or ATPase-defective rPrp22 (Figures 5L, 5M, 5R, and 5S; Figure S4C). For both an optimal and a suboptimal 3′ splice site, spliceosomes treated with rPrp22-K512A exhibited high FRET states, indicating juxtaposition of the 5′ exon and 3′ splice site in the exon ligation conformation (Figures 5K, 5L, 5N, 5Q, 5R, and 5T); the suboptimal 3′ splice site, like an optimal site (Figure 2M), also permitted juxtaposition of the 5′ exon and branch site in the exon ligation conformation (Figures S4D–S4F). For the optimal 3′ splice site substrate, wild-type rPrp22, relative to mutant, only slightly decreased the frequency of the high FRET state (Figures 5M and 5O). Importantly, for the suboptimal 3′ splice site, wild-type Prp22, relative to mutant, shifted a significant fraction of spliceosomes to a zero FRET state (Figures 5S and 5U), potentially equivalent to a zero FRET state previously observed for the same 3′ splice site mutant (Blanco et al., 2015). Thus, Prp22-dependent rejection before exon ligation promotes separation of potential reactants, just as Prp16 does before branching.

Evidence that Prp22 Translocates toward, but Not through, Its Target

Previously, we proposed that Prp22, as a 3′ to 5′ DEAH-box ATPase (Tanaka and Schwer, 2005), rejects a 3′ splice site or releases mRNA by translocating from the 3′ exon upstream to disrupt interactions between the substrate and the spliceosome (Mayas et al., 2006; see Introduction). Indeed, Prp22-dependent mRNA release requires at least 13 nt in the 3′ exon (Schwer, 2008). Thus, we tested whether truncation of a 3′ exon inhibited Prp22-dependent rejection of a 3′ splice site that competes with a second, downstream 3′ splice site (Figure 4). With a control substrate lacking the upstream 3′ splice site, truncation of the 3′ exon to 3 nt in length did not impact the efficiency of exon ligation at the downstream 3′ splice site (Figure 6A, lanes 1 and 2). However, in contrast to the full-length, tandem 3′ splice site substrate, which spliced at both 3′ splice sites (Figure 4B; Figure 6A, lane 3), a truncated, tandem 3′ splice site substrate spliced only at the upstream 3′ splice site (Figure 6A, lane 4). Thus, recognition of the downstream 3′ splice site, when in competition with the upstream 3′ splice site, required both Prp22 and substrate downstream, implying that Prp22 promotes 3′ splice site rejection, like mRNA release, by translocating from the 3′ exon in a 3′ to 5′ direction.

To test for evidence that Prp22, like Prp16, translocates toward, but not through, its target, we again substituted segments of the substrate with DNA, because the ATPase activity of Prp22 is similarly stimulated by ssRNA, but not ssDNA, and Prp22 cannot unwind a substrate with a 3′ ssDNA tail (Schwer, 2008; Tanaka and Schwer, 2005). Because substitutions in the intron and 3′ exon compromise Prp2 and Prp16 function, we could not investigate the impact of DNA substitutions on Prp22-mediated rejection of a 3′ splice site. Instead, we investigated the impact of DNA substitutions on Prp22-mediated release of mRNA using substrates substituted with DNA at regions flanking the exon-exon junction or within the 5′ exon (Figure 6B). By gradient fractionation of splicing reactions, unsubstituted mRNA released efficiently (71%), but mRNA substituted with DNA from −4 to +4 and from −8 to −1, relative to the exon-exon junction, did not (14% and 9%, respectively; Figure 6C). However, mRNAs substituted with DNA in the window of −9 to −2 did release efficiently (66%; Figure 6C) and in a Prp22-dependent manner (Figure S5A). Because the spliceosome footprints at least 13 nt of the 5′ exon just upstream from the exon-exon junction (Figure S5B; Schwer, 2008), these data do not support a model in which Prp22 must translocate through the mRNA-spliceosome interaction, although the data do suggest a requirement to translocate partially into the interaction.

To rule out that DNA substitutions impaired mRNA release by simply blocking recruitment rather than translocation of Prp22, we assayed for the impact of DNA substitution on the interaction between Prp22 and the 3′ exon established previously by s^4U crosslinking (Schwer, 2008). We supplemented Prp22-depleted extract with rPrp22-K512A, assembled spliceosomes on substrate substituted with s^4U at +17 relative to the exon-exon junction, and then induced crosslinking with UV (Figure 6D). With the all-RNA substrate, we observed a crosslink to Prp22 that we confirmed based on (1) migration at the expected molecular weight, (2) a dependence on substrate repositioning by Prp16 (Figure S5C), and (3) dependence on the presence of rPrp22-K512A (Figure 6D, lanes 2 with 4). Importantly, with the restrictive −4 to +4 DNA-substituted substrate, mutated rPrp22 crosslinked just as efficiently, in correlation with the extent of mRNA formed (Figure 6D, compare lanes 2 with 4 and 6 with 8). These data indicate that the −4 to +4 DNA substitution that blocked mRNA release did not block the interaction between Prp22 and the 3′ exon, implying that the DNA substitution instead blocked translocation of Prp22p upstream toward the exon-exon junction. Overall, our data are consistent with a model in which Prp22 translocates along the 3′ exon, moving the mRNA relative to the spliceosome to apply tension sufficient to disrupt substrate-spliceosome interactions.

DISCUSSION

During splicing, the spliceosome ensures specificity in selecting splice sites, but the mechanisms that facilitate splice site selection beyond spliceosome assembly have not been well understood. In this work, we establish that the DEAH-box ATPases Prp16 and Prp22 contribute to splice site selection at the catalytic stage (Figures 1 and 4). We also provide evidence that these ATPases antagonize the juxtaposition of splice sites, thereby rejecting suboptimal splice sites before they react and enabling substrate repositioning for exon ligation after branching

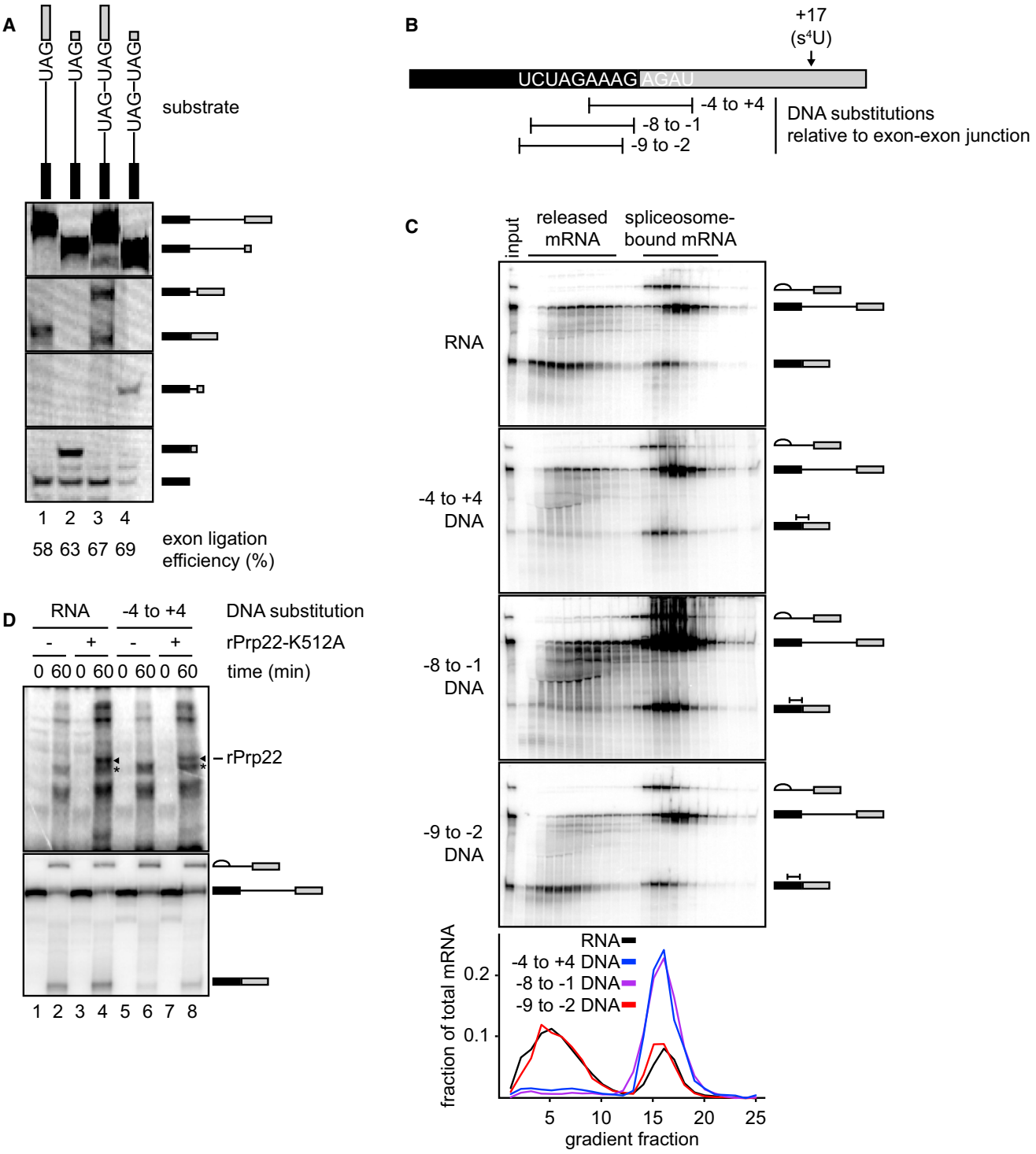

Figure 6. Prp22 Rearranges the Substrate by Translocating toward, but Not Necessarily through, Interactions with the Spliceosome

(A) Splicing of the indicated substrates was visualized via Cy5. The efficiency of branching was 4-fold lower in lane 4, but the efficiency of exon ligation was similar in all four lanes.

(B) Schematic of substrates with mRNA deoxy substitutions used in (C) and (D). Positions of the exon-exon junction and s^4U are indicated.

(C) Substrates with the indicated DNA substitutions were assayed for Prp22-dependent mRNA release.

(D) Substrates with or without the indicated DNA substitution and with the s^4U modification were incubated as indicated and then crosslinked. Crosslinking and splicing were monitored as in Figure 3E. Bands marked with an asterisk likely reflect crosslinking by Prp16.

See also Figure S5.

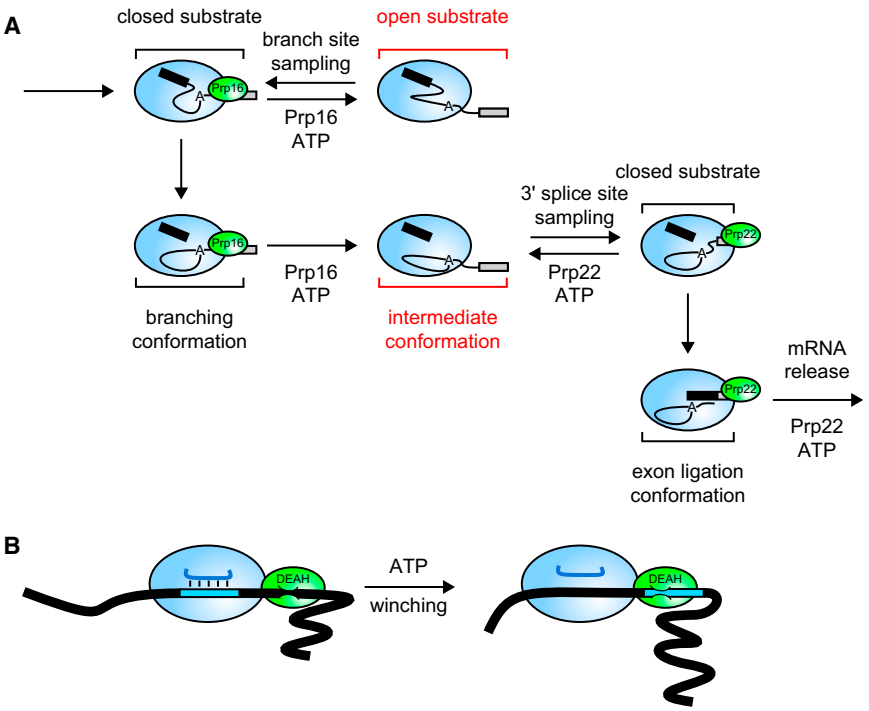

Figure 7. The Function and Mechanism of DEAH-Box ATPases at the Catalytic Stage of Splicing

(A) Prp16 and Prp22 function as chaperones for splice site selection by separating the splice sites. See text for details.

(B) A general winching model by which Prp16 and Prp22 promote spliceosomal rearrangements. See text for details.

See also Figure S6.

of optimal splice sites (Figures 2 and 5). Finally, we present evidence that these ATPases function through a mechanism involving translocation 3′ to 5′ along substrate RNA toward, but not through, their targets (Figures 3 and 6), suggesting that they disrupt interactions between the substrate and the spliceosome by limited translocation that manifests as pulling the substrate out of the catalytic core. Together, our data identify Prp16 and Prp22 as RNP chaperones that allow the spliceosome to search for splice sites (Figure 7A).

Just as a subset of RNA chaperones destabilize non-native ribozyme conformations to allow formation of an open conformation that then enables sampling of alternative conformations (Herschlag, 1995), Prp16 and Prp22 destabilize interactions between suboptimal splice sites and the spliceosome to promote formation of an open conformation (Figures 2, 5, and 7A), from which the spliceosome can sample alternative splice sites toward ultimately identifying an optimal splice site (Figure 7A). Indeed, our evidence that Prp16 disrupts the U2-branch site interaction rationalizes the Prp16-dependent proofreading of non-consensus branch sites (Burgess and Guthrie, 1993) that would bind U2 more weakly and unwind more readily. Additionally, like RNA chaperones, these DEAH-box ATPases enable escape from kinetic traps. For example, spliceosomes stalled on the d-brA substrate are stable for hours—until Prp16 acts (Figure 1). Further, just after branching, the spliceosome is kinetically trapped, unable to transition through an intermediate conformation to the exon ligation conformation (Ohrt et al., 2013)—until Prp16 acts. Our data indicate that Prp16 overcomes this kinetic trap by separating the 5′ splice site and branch site (Figure 2K), yielding an open conformation that then enables the spliceosome to sample the substrate for a 3′ splice site for exon ligation (Figures 2, 5, and 7A).

By demonstrating that Prp16-dependent rejection of a suboptimal branch site permits usage of alternative branch sites (Figures 1 and 7A), we provide insight into the recognition and rearrangement of the branch site during splicing. Although the U2-branch site helix can accommodate bulging of the nucleophile at multiple positions (Query et al., 1994; Smith et al., 2009), our data indicate that Prp16-dependent destabilization of the U2-branch site interaction is required for sampling of these alternative bulges (Figure 1D). We therefore conclude that U2 binds the branch site with the canonical adenosine bulged and fixes this register throughout assembly and catalytic activation of the spliceosome. Because alternative positions are selected as the nucleophile only after Prp16-dependent rejection, branch site selection must be less constrained after Prp16-dependent rejection than during assembly, though complementarity with U2 remains a requirement (Figure S1B). Importantly, genetic data have implicated parallel roles for Prp16 before and after branching and disruption of the U2-branch site helix before and after branching (Kannan et al., 2013; Semlow and Staley, 2012; Smith et al., 2007). The parallel between Prp16-dependent separation of the 5′ splice site and branch site before branching and of the 5′ exon and branch site afterward (Figure 2) supports a role for Prp16 in disrupting the U2-branch site interaction after branching, which provides a mechanism for branch site repositioning within the catalytic core to accommodate juxtaposition of the 5′ exon and 3′ splice site for exon ligation.

In addition to disrupting the U2-branch site interaction, Prp16 also promotes toggling of snRNA structures. Genetics have implicated Prp16 in the destabilization of U2/U6 helix Ia, which juxtaposes the 5′ splice site and branch site (Mefford and Staley, 2009). Indeed, Prp16 drove spliceosomes assembled on the BS-labeled substrate into a low FRET state nearly as low as the FRET state occupied by spliceosomes stalled before U4/U6 unwinding and U2/U6 helix Ia formation (compare Figures 2B and 2G). Disruption of this helix by Prp16 would facilitate separation of the 5′ splice site and a suboptimal branch site before branching and may result indirectly from disruption of the adjacent U2-branch site interaction. Genetics have also suggested that Prp16 promotes toggling of U2 from one conformation, stem IIc, to a mutually exclusive conformation, stem IIa

(Hilliker et al., 2007; Perriman and Ares, 2007). Given that U2 stem IIa is adjacent to the branch site binding region of U2, toggling to the stem IIa conformation may reposition the branch site binding region of U2 away from the branch site and facilitate sampling of alternative branch sites.

Our data suggest a model for Prp16-dependent remodeling of the U2-branch site interaction in which Prp16 disrupts the interaction from a distance (Figures 3 and 7B). In this model, Prp16 translocates along the substrate 3′ to 5′ from downstream of the catalytic core, but because Prp16 would remain anchored to the spliceosome, Prp16 would function as a molecular winch, moving the RNA substrate relative to the spliceosome, applying tension to the U2-branch site interaction and, ultimately, pulling the branch site off of U2. Importantly, this model provides a mechanism for unwinding a duplex that would otherwise be inaccessible to SF2 ATPases, such as DEAD-box ATPases (Ozgur et al., 2015), that require direct interaction with a duplex target.

Translocation along the substrate toward, but not necessarily through, interactions targeted for disruption, appears to be a general mechanism for DEAH-box ATPases at the catalytic stage of splicing. Prp22-dependent rejection of a 3′ splice site and mRNA release also requires substrate downstream of the catalytic core (Figure 6A; Schwer, 2008), consistent with a model in which Prp22 translocates from the 3′ exon upstream to disrupt interactions between the substrate and the spliceosome (Mayas et al., 2006). Further, our data indicate that Prp22-dependent mRNA release requires RNA upstream from its initial site of interaction with the 3′ exon but only up to the last nucleotide of the 5′ exon (Figures 6C and 6D). Thus, Prp22 can displace the spliceosome from mRNA without translocating entirely through interactions between the spliceosome and mRNA, interactions that extend ~15 nt upstream of the exon-exon junction. Prp22 and Prp16 may therefore share a common mechanism that involves loading onto substrate RNA downstream of the catalytic core and translocating to move the RNA substrate relative to the spliceosome, thereby pulling the substrate out of the catalytic core (Figure 7B). Consistent with a common mechanism, excess rPrp22 can partially substitute for Prp16 in chasing Prp16-depleted spliceosomes through exon ligation (Figure S6).

The mechanistic link between Prp22-dependent rejection of a 3′ splice site and recognition of an alternative 3′ splice site (Figures 4 and 6A) provides a basis for reconciling divergent views on the mechanism of 3′ splice site selection (Pérez-Valle and Vilardell, 2012). The exclusive selection of an upstream 3′ splice site over a downstream 3′ splice site in a bimolecular splicing assay has provided strong support for the proposal that the spliceosome employs a linear 5′ to 3′ scanning mechanism to identify the nearest 3′ splice site downstream of the branch site (Chen et al., 2000). Nevertheless, a 3′ splice site, if close to the branch site, lacking a strong polypyrimidine tract, or deviating from the consensus, can be skipped in favor of a downstream 3′ splice site, leading to the confounding conclusion that scanning can be "leaky" (Patterson and Guthrie, 1991; Smith et al., 1993) or that 3′ splice site selection is instead controlled by a diffusion-collision model (Umen and Guthrie, 1995). Our data indicate that Prp22 is required specifically for recognition of a downstream 3′ splice site (Figure 4) and can therefore account for the leaky feature of the scanning model and thereby support this model. We propose that the spliceosome scans to the first upstream 3′ splice site but that Prp22-dependent rejection can allow the spliceosome to dissociate the 3′ splice site and scan further downstream (Figure 4B). In our model, sequence determinants that disfavor an upstream site would sensitize the upstream 3′ splice site to Prp22-dependent rejection and facilitate scanning for downstream 3′ splice sites, a mechanism that could be targeted for regulation. Indeed, given that such DEAH-box ATPases are essential components of the splicing pathway, these factors are well positioned to control a wide variety of alternative splicing events. Further, given the breadth of this family of ATPases, they are similarly well positioned to control substrate specificity in a broad array of RNA-dependent processes.

EXPERIMENTAL PROCEDURES

See the Supplemental Experimental Procedures and Table S1 for details.

In Vitro Splicing and Isolation of Spliceosomal Intermediates

Splicing reactions containing 0.4 nM ^{32}P-labeled or 4 nM fluorescently labeled substrate (Abelson et al., 2010; Krishnan et al., 2013) were incubated at 20°C for 30–60 min under standard splicing conditions with 2 mM ATP and yeast whole-cell extract (Mayas et al., 2006) and inspected by denaturing PAGE. To stall spliceosomal intermediates for TIRF microscopy, yeast whole-cell extract was either immunodepleted of Prp16; supplemented with exogenous rPrp2-K252A, rPrp16-K379A, or rPrp22-K512A; or depleted of U6 and reconstituted with synthetic U6 containing the U80-PS(S_P) atomic substitution (Fica et al., 2013); assembled, but catalytically inactive, spliceosomes were stalled with a low ATP concentration of 0.1 mM (Tarn el al., 1993). Splicing reactions were separated on 15%–40% glycerol gradients and fractions containing spliceosomal intermediates were collected and stored at −80°C. Isolated spliceosomal intermediates were either directly immobilized for TIRF microscopy or first chased under standard splicing conditions with ATP, divalent metal, and/or exogenous splicing factors.

TIRF Microscopy

Stalled or chased spliceosomes were immobilized via biotinylated Prp19 or Prp8 that bound to streptavidin on the surface of polyethylene glycol-passivated quartz slides. Immobilized spliceosomes were washed to remove ATP and exogenous splicing factors and then imaged in splicing buffer lacking ATP. Single-molecule donor and acceptor emission trajectories were collected using a prism-based TIRF microscope with direct excitation of the donor fluorophore (Abelson et al., 2010). Presence of the acceptor fluorophore was confirmed by direct excitation. Individual donor and acceptor trajectories were filtered by visual inspection (Blanco and Walter, 2010), and then FRET values were calculated. Histograms describing the distribution of FRET values for a given population of spliceosomes were constructed by sampling the first ten frames of data (1 s total) from 103 to 1394 trajectories' for each spliceosome (Table S2). All reported changes in FRET distribution were observed in at least two independent spliceosome preparations.

Mapping the Branch Sites of Lariat Intermediates Formed by the br-dA Substrate

To map branch sites, 5′-^{32}P-labeled DNA primer (Table S1) was annealed to lariat intermediates and extended using avian myeloblastosis virus RT (Promega) in accordance with the manufacturer's instructions. Primer extension stops were inspected by denaturing PAGE.

UV Crosslinking

Splicing substrates were site specifically modified with s^{4}U and an associated ^{32}P radiolabel. Splicing reactions were irradiated with 365 nm UV and digested with RNase T1 before analysis.

mRNA Release Assays

Splicing reactions were incubated at 20°C for 60 min and then separated on 15%–40% glycerol gradients. Fractions were collected from the tops of gradients and inspected by denaturing PAGE.

SUPPLEMENTAL INFORMATION

Supplemental Information includes Supplemental Experimental Procedures, six figures, and two tables and can be found with this article online at http://dx.doi.org/10.1016/j.cell.2016.01.025.

AUTHOR CONTRIBUTIONS

D.R.S. and J.P.S. designed the experiments, interpreted the data, and wrote the paper with input from M.R.B. and N.G.W. D.R.S. generated reagents and performed all of the biochemistry experiments. D.R.S. and M.R.B. performed single-molecule FRET experiments. M.R.B. performed Gaussian fitting of histograms and statistical analysis of FRET trajectories.

ACKNOWLEDGMENTS

We thank B. Schwer and C. Guthrie for plasmids and antibodies, J. Abelson and C. Guthrie for sharing unpublished data, the members of the J.P.S. and N.G.W. laboratories for helpful discussions, especially S. Fica, M. Kahlscheuer, and R. Toroney, who also provided experimental assistance, and C. Guthrie, A. Hoskins, and J. Piccirilli for comments on the manuscript. D.R.S. and M.R.B. were supported by a Genetics and Regulation Training Grant (T32GM07197) and a Cellular and Molecular Biology Training Grant (T32GM007315), respectively, both from the NIH. This work was funded by grants from the NIH (R01GM062264 and R01GM062264-08S1 to J.P.S.; R01GM098023 to N.G.W.).

Received: July 23, 2014
Revised: January 8, 2016
Accepted: January 15, 2016
Published: February 25, 2016

REFERENCES

Abelson, J., Blanco, M., Ditzler, M.A., Fuller, F., Aravamudhan, P., Wood, M., Villa, T., Ryan, D.E., Pleiss, J.A., Maeder, C., et al. (2010). Conformational dynamics of single pre-mRNA molecules during in vitro splicing. Nat. Struct. Mol. Biol. *17*, 504–512.

Blanco, M., and Walter, N.G. (2010). Analysis of complex single-molecule FRET time trajectories. Methods Enzymol. *472*, 153–178.

Blanco, M.R., Martin, J.S., Kahlscheuer, M.L., Krishnan, R., Abelson, J., Laederach, A., and Walter, N.G. (2015). Single Molecule Cluster Analysis dissects splicing pathway conformational dynamics. Nat. Methods *12*, 1077–1084.

Burgess, S.M., and Guthrie, C. (1993). A mechanism to enhance mRNA splicing fidelity: the RNA-dependent ATPase Prp16 governs usage of a discard pathway for aberrant lariat intermediates. Cell *73*, 1377–1391.

Chen, S., Anderson, K., and Moore, M.J. (2000). Evidence for a linear search in bimolecular 3′ splice site AG selection. Proc. Natl. Acad. Sci. USA *97*, 593–598.

Chua, K., and Reed, R. (1999). The RNA splicing factor hSlu7 is required for correct 3′ splice-site choice. Nature *402*, 207–210.

Company, M., Arenas, J., and Abelson, J. (1991). Requirement of the RNA helicase-like protein PRP22 for release of messenger RNA from spliceosomes. Nature *349*, 487–493.

Crawford, D.J., Hoskins, A.A., Friedman, L.J., Gelles, J., and Moore, M.J. (2013). Single-molecule colocalization FRET evidence that spliceosome activation precedes stable approach of 5′ splice site and branch site. Proc. Natl. Acad. Sci. USA *110*, 6783–6788.

Fica, S.M., Tuttle, N., Novak, T., Li, N.S., Lu, J., Koodathingal, P., Dai, Q., Staley, J.P., and Piccirilli, J.A. (2013). RNA catalyses nuclear pre-mRNA splicing. Nature *503*, 229–234.

Hang, J., Wan, R., Yan, C., and Shi, Y. (2015). Structural basis of pre-mRNA splicing. Science *349*, 1191–1198.

Herschlag, D. (1995). RNA chaperones and the RNA folding problem. J. Biol. Chem. *270*, 20871–20874.

Hilliker, A.K., Mefford, M.A., and Staley, J.P. (2007). U2 toggles iteratively between the stem IIa and stem IIc conformations to promote pre-mRNA splicing. Genes Dev. *21*, 821–834.

James, S.A., Turner, W., and Schwer, B. (2002). How Slu7 and Prp18 cooperate in the second step of yeast pre-mRNA splicing. RNA *8*, 1068–1077.

Jankowsky, E. (2011). RNA helicases at work: binding and rearranging. Trends Biochem. Sci. *36*, 19–29.

Kannan, R., Hartnett, S., Voelker, R.B., Berglund, J.A., Staley, J.P., and Baumann, P. (2013). Intronic sequence elements impede exon ligation and trigger a discard pathway that yields functional telomerase RNA in fission yeast. Genes Dev. *27*, 627–638.

Koodathingal, P., Novak, T., Piccirilli, J.A., and Staley, J.P. (2010). The DEAH box ATPases Prp16 and Prp43 cooperate to proofread 5′ splice site cleavage during pre-mRNA splicing. Mol. Cell *39*, 385–395.

Krishnan, R., Blanco, M.R., Kahlscheuer, M.L., Abelson, J., Guthrie, C., and Walter, N.G. (2013). Biased Brownian ratcheting leads to pre-mRNA remodeling and capture prior to first-step splicing. Nat. Struct. Mol. Biol. *20*, 1450–1457.

Mayas, R.M., Maita, H., and Staley, J.P. (2006). Exon ligation is proofread by the DExD/H-box ATPase Prp22p. Nat. Struct. Mol. Biol. *13*, 482–490.

Mayas, R.M., Maita, H., Semlow, D.R., and Staley, J.P. (2010). Spliceosome discards intermediates via the DEAH box ATPase Prp43p. Proc. Natl. Acad. Sci. USA *107*, 10020–10025.

McPheeters, D.S., and Muhlenkamp, P. (2003). Spatial organization of protein-RNA interactions in the branch site-3′ splice site region during pre-mRNA splicing in yeast. Mol. Cell. Biol. *23*, 4174–4186.

Mefford, M.A., and Staley, J.P. (2009). Evidence that U2/U6 helix I promotes both catalytic steps of pre-mRNA splicing and rearranges in between these steps. RNA *15*, 1386–1397.

Ohrt, T., Prior, M., Dannenberg, J., Odenwälder, P., Dybkov, O., Rasche, N., Schmitzová, J., Gregor, I., Fabrizio, P., Enderlein, J., and Lührmann, R. (2012). Prp2-mediated protein rearrangements at the catalytic core of the spliceosome as revealed by dcFCCS. RNA *18*, 1244–1256.

Ohrt, T., Odenwälder, P., Dannenberg, J., Prior, M., Warkocki, Z., Schmitzová, J., Karaduman, R., Gregor, I., Enderlein, J., Fabrizio, P., and Lührmann, R. (2013). Molecular dissection of step 2 catalysis of yeast pre-mRNA splicing investigated in a purified system. RNA *19*, 902–915.

Ozgur, S., Buchwald, G., Falk, S., Chakrabarti, S., Prabu, J.R., and Conti, E. (2015). The conformational plasticity of eukaryotic RNA-dependent ATPases. FEBS J. *282*, 850–863.

Patterson, B., and Guthrie, C. (1991). A U-rich tract enhances usage of an alternative 3′ splice site in yeast. Cell *64*, 181–187.

Pérez-Valle, J., and Vilardell, J. (2012). Intronic features that determine the selection of the 3′ splice site. Wiley Interdiscip. Rev. RNA *3*, 707–717.

Perriman, R.J., and Ares, M., Jr. (2007). Rearrangement of competing U2 RNA helices within the spliceosome promotes multiple steps in splicing. Genes Dev. *21*, 811–820.

Prabu, J.R., Müller, M., Thomae, A.W., Schüssler, S., Bonneau, F., Becker, P.B., and Conti, E. (2015). Structure of the RNA helicase MLE reveals molecular mechanisms for uridine specificity and RNA-ATP coupling. Mol. Cell *60*, 487–499.

Query, C.C., Moore, M.J., and Sharp, P.A. (1994). Branch nucleophile selection in pre-mRNA splicing: evidence for the bulged duplex model. Genes Dev. *8*, 587–597.

Schwer, B. (2008). A conformational rearrangement in the spliceosome sets the stage for Prp22-dependent mRNA release. Mol. Cell *30*, 743–754.

Schwer, B., and Guthrie, C. (1991). PRP16 is an RNA-dependent ATPase that interacts transiently with the spliceosome. Nature *349*, 494–499.

Semlow, D.R., and Staley, J.P. (2012). Staying on message: ensuring fidelity in pre-mRNA splicing. Trends Biochem. Sci. *37*, 263–273.

Smith, C.W., Chu, T.T., and Nadal-Ginard, B. (1993). Scanning and competition between AGs are involved in 3′ splice site selection in mammalian introns. Mol. Cell. Biol. *13*, 4939–4952.

Smith, D.J., Query, C.C., and Konarska, M.M. (2007). trans-splicing to spliceosomal U2 snRNA suggests disruption of branch site-U2 pairing during pre-mRNA splicing. Mol. Cell *26*, 883–890.

Smith, D.J., Konarska, M.M., and Query, C.C. (2009). Insights into branch nucleophile positioning and activation from an orthogonal pre-mRNA splicing system in yeast. Mol. Cell *34*, 333–343.

Tanaka, N., and Schwer, B. (2005). Characterization of the NTPase, RNA-binding, and RNA helicase activities of the DEAH-box splicing factor Prp22. Biochemistry *44*, 9795–9803.

Tarn, W.-Y., Lee, K.-R., and Cheng, S.-C. (1993). Yeast precursor mRNA processing protein PRP19 associates with the spliceosome concomitant with or just after dissociation of U4 small nuclear RNA. Proc. Natl. Acad. Sci. USA *90*, 10821–10825.

Umen, J.G., and Guthrie, C. (1995). The second catalytic step of pre-mRNA splicing. RNA *1*, 869–885.

Villa, T., and Guthrie, C. (2005). The Isy1p component of the NineTeen complex interacts with the ATPase Prp16p to regulate the fidelity of pre-mRNA splicing. Genes Dev. *19*, 1894–1904.

Wahl, M.C., Will, C.L., and Lührmann, R. (2009). The spliceosome: design principles of a dynamic RNP machine. Cell *136*, 701–718.

Wang, Y., Wagner, J.D., and Guthrie, C. (1998). The DEAH-box splicing factor Prp16 unwinds RNA duplexes in vitro. Curr. Biol. *8*, 441–451.

Warkocki, Z., Schneider, C., Mozaffari-Jovin, S., Schmitzová, J., Höbartner, C., Fabrizio, P., and Lührmann, R. (2015). The G-patch protein Spp2 couples the spliceosome-stimulated ATPase activity of the DEAH-box protein Prp2 to catalytic activation of the spliceosome. Genes Dev. *29*, 94–107.

Wlodaver, A.M., and Staley, J.P. (2014). The DExD/H-box ATPase Prp2p destabilizes and proofreads the catalytic RNA core of the spliceosome. RNA *20*, 282–294.

Supplemental Figures

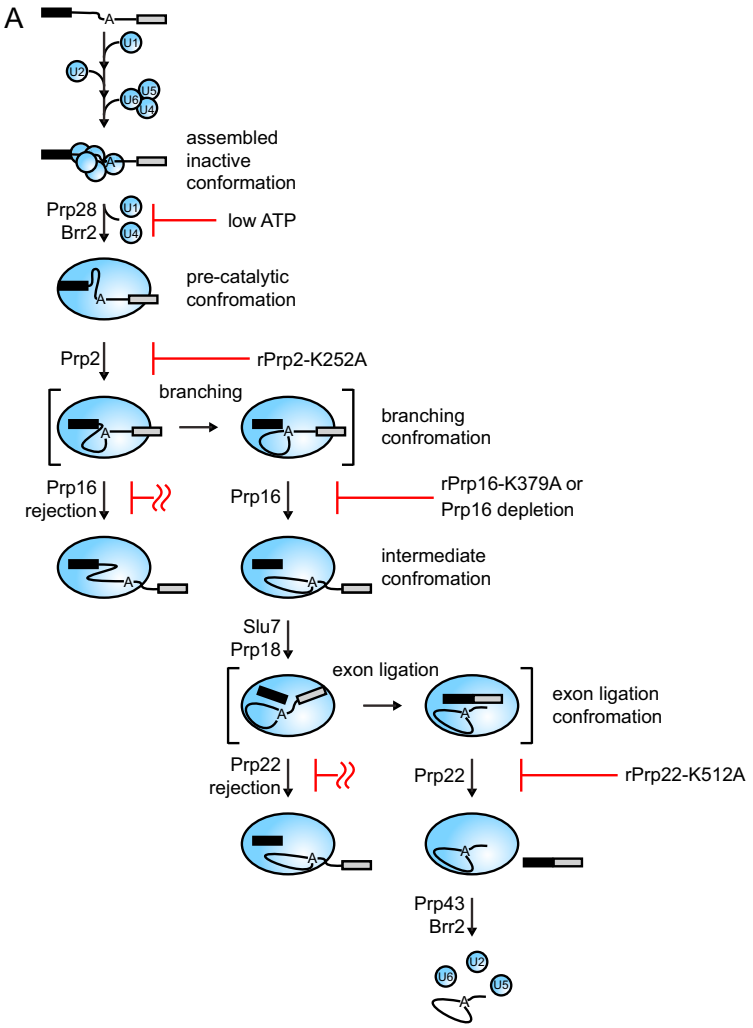

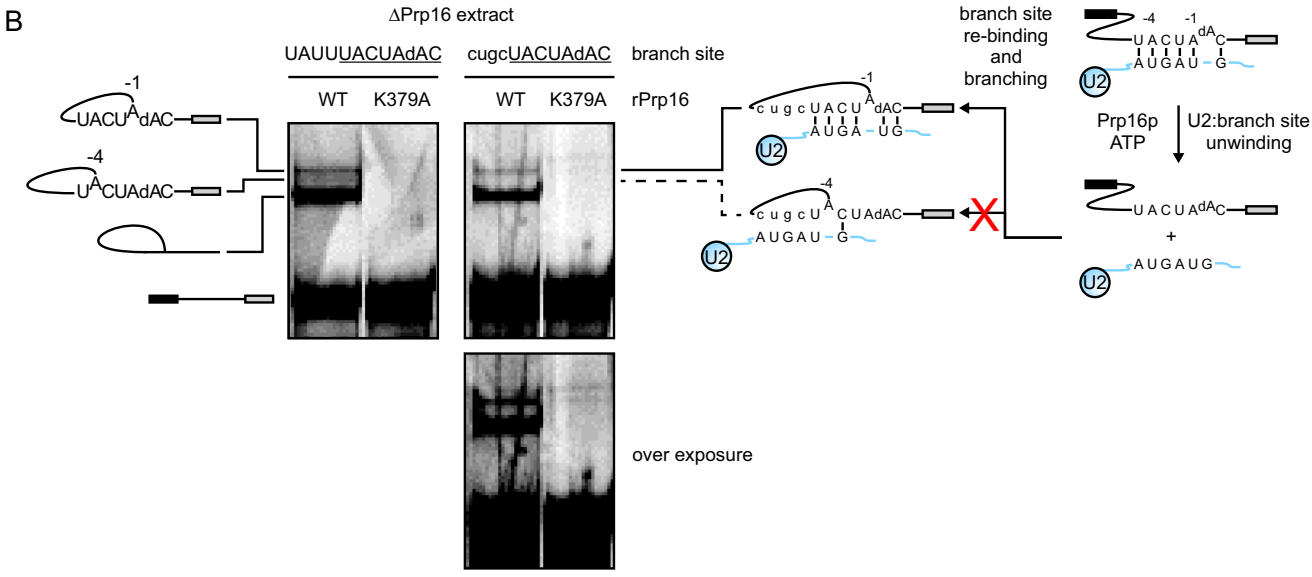

(legend on next page)

Figure S1. Diagram of the Splicing Pathway and Evidence that Alternative Branch Site Selection Requires Complementarity to U2, Related to Figure 1

(A) See main text for details. Small blue circles represent small nuclear RNPs; large blue ovals represent the compositionally mature spliceosome. In this work, specific transitions were blocked by limiting the ATP concentration in extract (Tarn et al., 1993) or adding a dominant-negative, mutated DEAH-box ATPase (Hotz and Schwer, 1998; Schwer and Gross, 1998; this work), as indicated; the transition to exon ligation was also blocked by immunodepletion of Prp16 (Schwer, 2008).

(B) Splicing substrates with either a *UAUU*<u>*UAC*</u>UAdAC or *cugc*<u>*UAC*</u>UAdAC branch site were incubated in Prp16-depleted extract supplemented with wild-type or mutated rPrp16. Note that the *cugc*<u>*UAC*</u>UAdAC substrate has reduced complementarity to U2 relative to the *UAUU*<u>*UAC*</u>UAdAC control substrate in the italicized register that we hypothesized necessary for branching from the −4 adenosine (the canonical branch site register is underlined). Accordingly, a faster migrating lariat intermediate species, consistent with splicing at −4 relative to the canonical branch site (left), is not detected for the *cugc*<u>*UAC*</u>UAdAC substrate (right). The inferred activity of Prp16 is modeled in the cartoon.

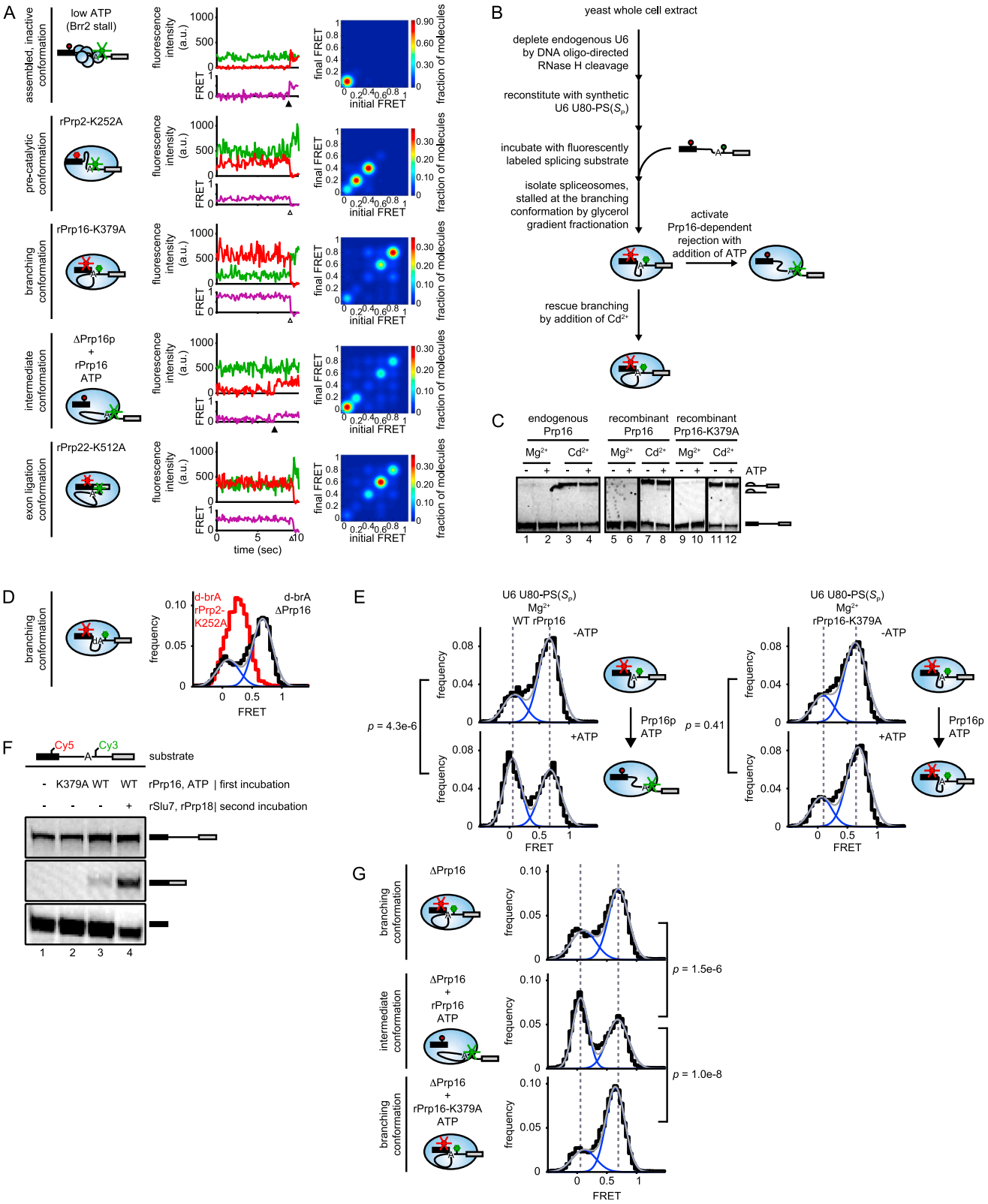

(legend on next page)

Figure S2. Separation of the 5′ Exon and Branch Site Both before and after Branching Requires the ATPase Activity of Prp16, Related to Figure 2

(A) Spliceosomes were assembled on BS-labeled substrate, stalled as indicated, isolated by gradient fractionation, and immobilized for TIRF microscopy. Representative donor, acceptor, and FRET trajectories (left) are shown for the indicated spliceosomal populations. Transition occupancy density plots (TODPs; right; Blanco and Walter, 2010) illustrate the fraction of spliceosomes that undergo a transition from a given initial FRET state to a given final FRET state. Molecules that occupied only one FRET state, and thus did not transition, are revealed on the diagonal at the position of the occupied FRET state. As observed previously for a subset of stalled spliceosomal intermediates (Krishnan et al., 2013), the FRET states were generally static with a minimum of 79% FRET trajectories exhibiting no FRET transitions over the window of observation (4 to 60 s; Table S2). See the methods section for further description.

(B) Experimental strategy for assaying Prp16-dependent rejection with spliceosomes that were assembled on BS-labeled substrate and stalled by the U6 U80-PS(S_P) atomic substitution.

(C) U6 U80-PS(S_P)-stalled spliceosomes assembled on BS-labeled substrates undergo branching in the presence of thiophilic metal (Fica et al., 2013; Koodathingal et al., 2010; Yean et al., 2000). U6 U80-PS(S_P)-stalled spliceosomes isolated as in (B) from extract containing only endogenous Prp16 (lanes 1-4) or supplemented with wild-type rPrp16 (lanes 5-8) or rPrp16-K379A (lanes 9-12) and then incubated with divalent metal with or without ATP as indicated. Note that while Mg^{2+} has previously supported branching of U80-PS(S_P)-stalled spliceosomes in the absence of ATP with a longer, non-fluorescently labeled, enzymatically produced *UBC4* transcript (Koodathingal et al., 2010), Mg^{2+} did not support branching in the absence of ATP with this shorter, synthetic, fluorescently labeled substrate, possibly due to the fluorophores positioned near the 5′ splice site and branch site. Nevertheless, Mg^{2+} did permit splice site juxtaposition of the fluorescently labeled substrate in the branching conformation (Figures 2F and S2E, top). Given our experimental goal of testing the impact of Prp16 on splice site juxtaposition during proofreading before branching, inefficient branching in Mg^{2+} served as an advantage, because it allowed us to uncouple proofreading from branching.

(D) FRET distribution for Prp16-depleted spliceosomes that were assembled on the BS-labeled d-brA substrate and isolated by gradient fractionation. The FRET distribution for rPrp2-K252A-stalled spliceosomes assembled on d-brA substrates is included for reference (red). The FRET distribution for Prp16-depleted spliceosomes that were assembled on d-brA substrate indicates stalling in the 5′ splice site cleavage conformation (cf. Figure 2D).

(E) FRET distributions for U6 U80-PS(S_P)-stalled spliceosomes assembled in extract supplemented with wild-type rPrp16 (left) or rPrp16-K379A (right) and imaged before (top) or after (bottom) activation of Prp16-dependent proofreading with addition of ATP.

(F) Spliceosomes stalled after branching by Prp16 depletion and isolated by gradient fractionation were chased through exon ligation by a first incubation with ATP and rPrp16 for 20 min followed by a second incubation with rSlu7 and rPrp18 for an additional 20 min. Splicing was visualized via Cy5.

(G) ATPase-defective rPrp16-K379A fails to shift spliceosomes to the near-zero FRET state. Prp16-depleted spliceosomes were isolated and chased as in (F). The top and middle panels are reproduced from Figure 2, J and K for comparison. Histograms were fit as in Figure 2. p values were determined as in Figure 2.

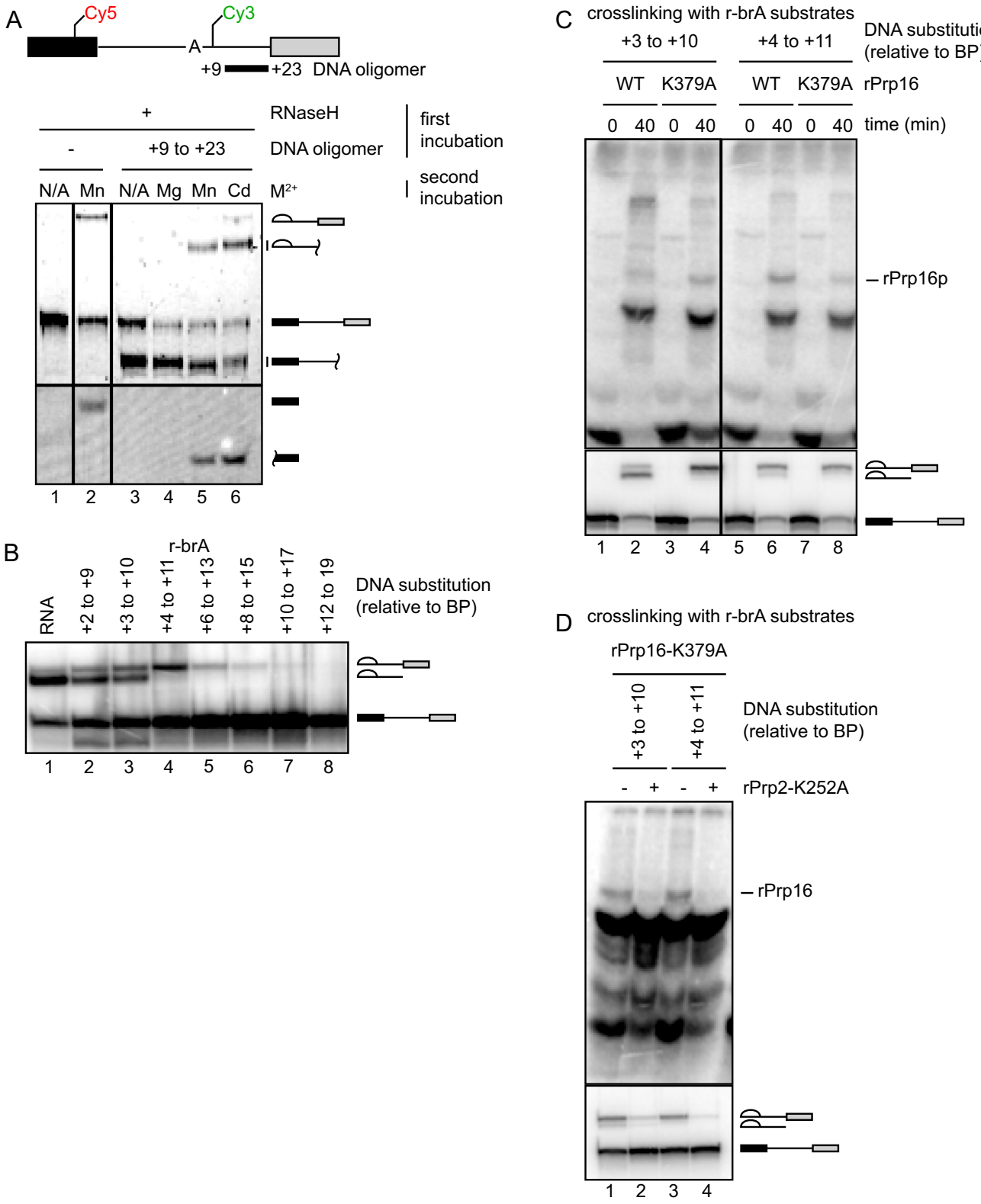

Figure S3. Prp16 Interacts with the Splicing Substrate Downstream of the Branch Site Specifically at the Branching Stage, Related to Figure 3

(A) Substrate cleavage downstream of the branch site does not impede the branching reaction. U6 U80-PS(S_P)-stalled spliceosomes were assembled on r-brA BS-labeled substrate, isolated by gradient fractionation, and site-specifically cleaved by DNA oligomer-directed RNase H. The sample was then split and either

(legend continued on next page)

quenched or assayed for chase through branching after the addition of Mg^{2+}, Mn^{2+}, or Cd^{2+}, as indicated. Diagram indicates region of the substrate complementary to the DNA oligomer with positions numbered relative to the branchpoint. Pre-mRNA and lariat intermediates were visualized via Cy3; 5′ exon was visualized via Cy5. Note that the DNA oligomer hybridizes 1 to 4 nts closer to the active branch site nucleotide in this r-brA substrate than to the active branch site nucleotides in the d-brA substrate (Figure 3A), so this control is particularly stringent. Also note that cleavage induced by this oligomer already suggests that the corresponding region of the substrate is unprotected in the branching conformation of the spliceosome. Further note that although the fraction of uncleaved pre-mRNA decreased during the chase (compare lane 3 with lanes 4, 5, and 6), in Cd^{2+}, for example, the fraction of cleaved pre-mRNA decreased twice as much and splicing intermediates increased three times as much (lane 6); additionally, the uncleaved pre-mRNA in Mg^{2+} also decreased, but no intermediates were observed (lane 4). Thus, the majority of free 5′ exon and cleaved lariat intermediate derived from the cleaved pre-mRNA. Lastly, note that in lanes treated with DNA oligomer and thiophilic metal, the free 5′ exon migrated faster than expected, consistent with a free 5′ exon that is 4 nt shorter (compare lane 2 with lanes 5 and 6). This faster migration is likely due to off-target RNaseH cleavage given complementarity between the DNA oligomer and the first 6 nts of the 5′ exon (Table S1).

(B) Splicing of substrates with the indicated 8 nt DNA substitutions was performed in yeast extract. DNA substitutions between +6 and +19 relative to the branch site (lanes 5 to 8) compromised branching, most likely by impeding the function of the DEAH-box ATPase Prp2. This inference is consistent with previous work that demonstrated a requirement for substrate RNA 23 to 33 nt downstream of the branch site at the Prp2p stage (Liu and Cheng, 2012; Warkocki et al., 2015).

(C) Splicing of substrates with the indicated DNA substitutions and a 4-thio-uracil modification 18 nt downstream of the branch site were spliced in Prp16-depleted extract supplemented with wild-type (WT) or mutated (K379A) rPrp16. Crosslinking was activated by UV irradiation and transfer of an RNA radiolabel to protein was assayed by SDS-PAGE, after digestion with RNase T1. Note that accumulation of a radiolabeled band consistent with Prp16 correlates with formation of lariat intermediate (compare lanes 1 and 2, 3 and 4, 5 and 6, and 7 and 8). Also note that in the presence of wild-type rPrp16, the Prp16 crosslink accumulates to a greater extent for the non-permissive +4 to +11 DNA substituted substrate than for the permissive +3 to +10 DNA substituted substrate, consistent with increased accumulation of lariat intermediate for the +4 to +11 DNA substituted substrate (compare lanes 2 and 6). The apparent decrease of the crosslink in lane 8 versus lane 6 was not observed in replicate experiments. These observations corroborate the assignment of the noted crosslinked band to Prp16 and provide further evidence that Prp16 interacts with the substrate specifically at (but not after) the branching stage of splicing.

(D) Splicing and crosslinking was performed as in (C) with extract supplemented with mutated rPrp16-K379A and either buffer or rPrp2-K252A. In the presence of rPrp2-K252A, which blocks branching (bottom; Figure S1A), the rPrp16 crosslink fails to accumulate (compare lanes 1 and 2 and lanes 3 and 4), implying that crosslinking to the substrate by rPrp16 depends on formation of the branching conformation of the spliceosome.

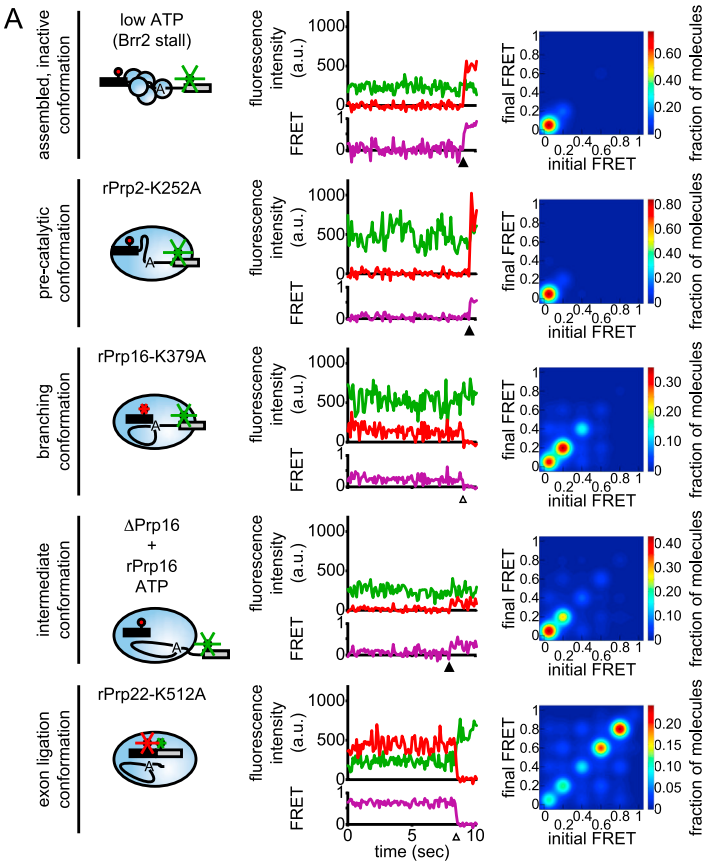

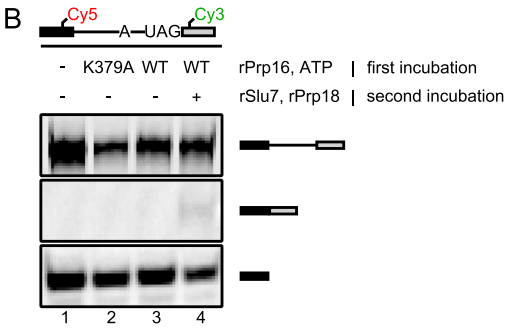

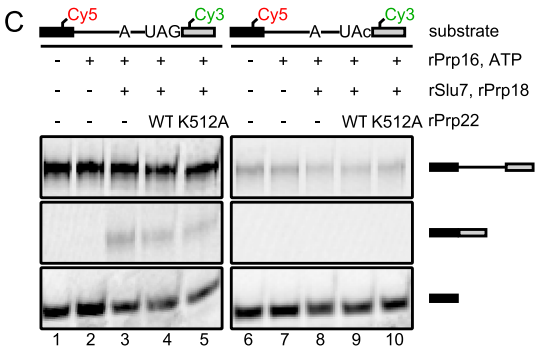

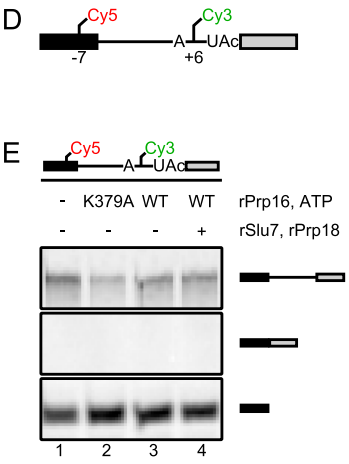

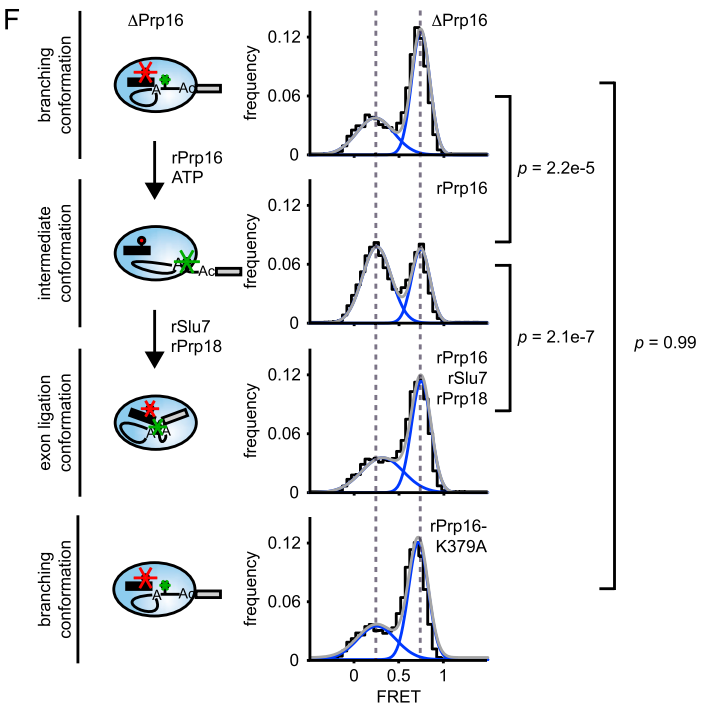

(legend on next page)

Figure S4. A Suboptimal 3′ Splice Site Permits Juxtaposition of the 5′ Splice Site with Both the Branch Site and 3′ Splice Site at Exon Ligation, Related to Figure 5

(A) Spliceosomes were assembled on 3'SS-labeled substrate, stalled as indicated, isolated by gradient fractionation, and immobilized for TIRF microscopy. Representative donor, acceptor, and FRET trajectories (left data panels) are shown for the indicated spliceosomal populations. Transition occupancy density plots (TODPs; right data panels; Blanco and Walter, 2010) illustrate the fraction of spliceosomes that undergo a transition from a given initial FRET state to a given final FRET state. Molecules that occupied only one FRET state, and thus did not transition, are revealed on the diagonal at the position of the occupied FRET state. More than 77% of all molecules in each plot were static (Table S2). See the Experimental Procedures for further description.

(B) Spliceosomes that were stalled after branching by Prp16-depletion and then isolated by gradient fractionation were chased through exon ligation by a first incubation with ATP and rPrp16 for 20 min followed by a second incubation with rSlu7 and rPrp18 for an additional 20 min. Splicing was visualized via Cy5. Note that in this representative panel, as for the left panel in (C) below, the pre-mRNA levels for the UAG reactions were elevated due to selection of a denser gradient fraction that consequently included a higher percentage of pre-mRNA-containing spliceosomes; however, gradient fractions ultimately used for TIRF microscopy contained lower levels of pre-mRNA. Note also that mRNA in lane 4 is underrepresented due to a diffuse mRNA migration pattern observed with the 3'SS-labeled substrate; exon ligation is also reflected in the reduced 5' exon levels.

(C) Prp16-depleted spliceosomes assembled on substrate with labels at the 5' and 3' splice sites were isolated by gradient fractionation and then chased into the exon ligation conformation by addition of ATP and the factors indicated.

(D) Schematic of synthetic substrate with a suboptimal (UAc) 3' splice site and fluorescently labeled at the 5' splice site and the branch site.

(E) Prp16-depleted spliceosomes assembled on substrate with labels at the 5' splice site and branch site were isolated by gradient fractionation and then chased into the exon ligation conformation by addition of ATP and the factors indicated. Note that although we and others have previously observed that substrates with a suboptimal UAc 3' splice site undergo exon ligation in the absence of ATP or in the presence of an ATPase-deficient rPrp22 mutant in the context of an *ACT1* splicing substrate (Mayas et al., 2006; Tseng and Cheng, 2008), the *UBC4* UAc substrates used in this study do not undergo exon ligation in the absence of ATP or the presence of a rPrp22 mutant, due at least in part to positioning of the FRET acceptor and donor near the 5' splice site and 3' splice site or branch site, respectively. Given our experimental goal of testing the impact of Prp22 on splice site juxtaposition during proofreading before exon ligation, inefficient exon ligation served as an advantage, because it allowed us to uncouple proofreading from exon ligation.

(F) The 5' splice site and branch site are juxtaposed for exon ligation in the presence of a suboptimal 3' splice site. FRET distributions for spliceosomes that were assembled on BS-labeled substrate with a suboptimal 3' splice site, stalled by Prp16-depletion, and chased as in (E). rPrp16 drove spliceosomes from a high FRET state into a low FRET state, indicating that rPrp16 separated the 5' splice site and branch site, as with an optimal 3' splice site substrate (Figures 2J, 2K, and 2N). rSlu7 and rPrp18 shifted spliceosomes back to a high FRET state, indicating that juxtaposition of the 5' splice site and branch site for exon ligation occurs even for a substrate with a suboptimal UAc 3' splice site, as with an optimal 3' splice site substrate (Figures 2K–2M and 2O). This juxtaposition of the 5' splice site and branch site parallels juxtaposition of the 5' splice site and the suboptimal 3' splice site itself, from the perspective of the 3' splice site label (Figures 5Q, 5R, and 5T), indicating coordinated juxtaposition of the 5' splice site with the branch site and 3' splice site in the exon ligation conformation for a substrate with a suboptimal UAc 3' splice site, as with an optimal 3' splice site substrate (Figures 2K–2M and 2O; Figures 5F–5H and 5J). Histograms were fit as in Figure 2. p values were determined as in Figure 2.

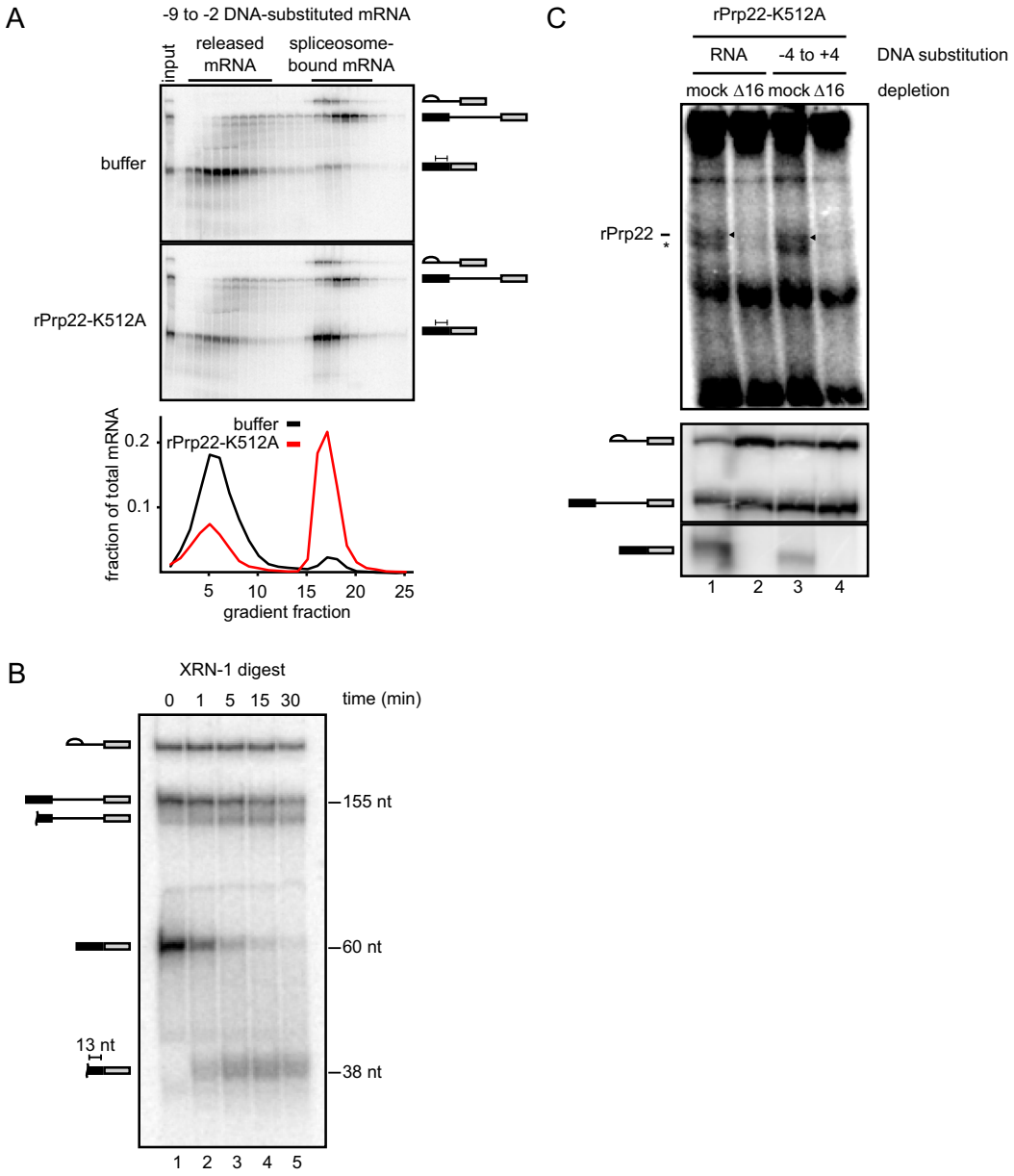

Figure S5. Prp22 Promotes Release of a DNA-Substituted mRNA and Associates with the 3′ Exon at Exon Ligation Even in the Absence of mRNA Release, Related to Figure 6

(A) mRNA release of a substrate with a permissive DNA substitution requires Prp22. Substrate with a DNA substitution from −9 to −2 relative to the exon-exon junction was spliced in yeast extract supplemented with buffer (top) or rPrp22-K512A (middle) and the mRNA was assayed for Prp22-dependent release from the spliceosome by glycerol gradient fractionation. The amount of mRNA present in each gradient fraction relative to the total mRNA level is quantitated (bottom).

(B) Spliceosomes assembled on a substrate with a 35 nt 5′ exon and 25 nt 3′ exon were stalled just after mRNA formation with rPrp22-K512A, isolated by gradient fractionation, and then digested with the 5′ to 3′ exonuclease XRN-1. The digested RNA was analyzed by PAGE. Note that a 38 nt fragment derived from mRNA is produced by XRN-1 digestion, indicating protection of 13 nt of the 5′ exon by the spliceosome.

(C) Splicing of substrates lacking (lanes 1 and 2) or having (lanes 3 and 4) a DNA substitution that is non-permissive for mRNA release and a 4-thio-uracil modification 17 nt downstream of the exon-exon junction were spliced in mock-depleted (mock; lanes 1 and 3) or Prp16-depleted (Δ16; lanes 2 and 4) extract supplemented with mutated rPrp22-K512A. Crosslinking was activated by UV irradiation and transfer of an RNA radiolabel to protein was assayed by SDS-PAGE, after digestion with RNase T1. Accumulation of a radiolabeled band consistent with Prp22 (marked by arrowheads) correlates with formation of mRNA (compare lanes 1 and 2 and lanes 3 and 4), implying that crosslinking to the substrate by Prp22 is specific for spliceosomes that have reached the exon ligation conformation. Bands marked with an asterisk likely reflect crosslinking by Prp16.

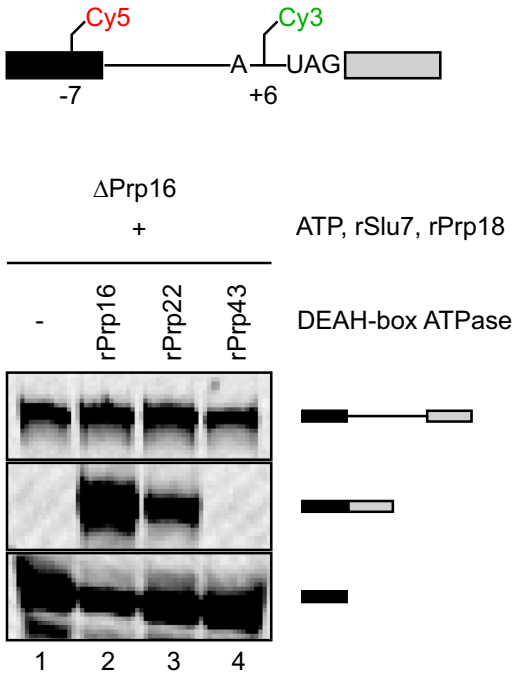

Figure S6. In a Purified System, Prp22 Can Partially Substitute for Prp16 in Promoting Exon Ligation, Related to Figure 7

Spliceosomes were assembled on BS-labeled substrate, stalled after branching by Prp16 depletion, isolated by gradient fractionation, and then chased through exon ligation upon addition of ATP and the indicated factors. As with the addition of rPrp16, addition of rPrp22, at high concentration and in conjunction with rSlu7 and rPrp18, stimulated mRNA formation. By contrast, addition of the spliceosomal DEAH-box ATPase rPrp43 did not support exon ligation, indicating that any DEAH-box ATPase is not sufficient.

Cell, Volume *164*

Supplemental Information

Spliceosomal DEAH-Box ATPases Remodel Pre-mRNA to Activate Alternative Splice Sites

Daniel R. Semlow, Mario R. Blanco, Nils G. Walter, and Jonathan P. Staley

Supplemental Experimental Procedures

Yeast Strains

The assembled but inactive spliceosomal intermediate (Figure S1) was assembled from extracts of an *S. cerevisiae* strain (yJPS1493) that expresses Prp8 with a C-terminal biotinylation signal that is a substrate for endogenous biotin ligase. This strain was derived from BY4741 (*MAT**a** his3Δ1 leu2Δ0 met15Δ0 ura3Δ0*, Open Biosystems) by replacing the stop codon of the chromosomal *PRP8* locus with a PCR fragment amplified from pFA6-HTB-kanMX6 (Tagwerker et al., 2006) that contained the biotinylation signal, *ADH1* terminator, and *kanMX6* selectable marker. All other spliceosomal intermediates (Figure S1) were assembled from extracts of yJPS1405, which expresses Prp19 with a C-terminal biotinylation signal (Fica et al., 2013).

Synthesis of Splicing Substrates

UBC4-derived substrates (Table S1) were prepared as described previously (Abelson et al., 2010) with modifications. Oligonucleotides (Thermo Scientific and Integrated DNA Technologies) were deprotected and gel purified. For FRET studies, oligonucleotides containing 5-aminoallyluridine at specific positions were conjugated to fluorophores by incubation with a 20-fold excess of Cy3 or Cy5 CyDye N-hydroxysuccinimidyl ester (GE) for 30 min at 60 °C in 0.1 M sodium carbonate buffer (pH 8.5). Fluorescently labeled oligonucleotides were separated from unincorporated dye by ethanol precipitation followed by repeated washing with 70% ethanol. Cy5-labeled oligonucleotide was separated from unlabeled oligonucleotide by reversed phase HPLC using a C18 column and eluted on a 10-25% acetonitrile gradient. Cy3-labeled oligonucleotide was separated from unlabeled oligonucleotide using a gravity flow benzoylated naphthoylated DEAE-cellulose (Sigma) column and eluted with 1.5 M NaCl in 20% ethanol. For non-fluorescent substrates, oligonucleotides were 5' end radiolabeled using [γ-^{32}P] ATP and T4

PNK (Thermo Scientific) according to the manufacturer's protocol. Following labeling, oligonucleotides were then joined to generate the full-length substrates by splinted ligation using T4 DNA ligase (New England Biolabs) and DNA splints (Integrated DNA Technologies) with 20 nucleotides complementarity on each side of the ligation junctions, as described previously (Abelson et al., 2010). For historical reasons, the tandem 3' splice site substrate contained a sulfur substitution of the *pro*-S_P phosphate oxygen at the upstream 3' splice site (UAG-PS[S_P]-AACUAG), which does not significantly affect exon ligation (Fica et al., 2013). To generate this substrate, a fourteen nucleotide RNA oligomer containing the *pro*-S_P phosphate oxygen substitution was first isolated from a mixture of diastereomers by reversed phase HPLC using a C18 column and eluted on a 4-9% acetonitrile gradient (Frederiksen and Piccirilli, 2009). The stereochemically pure 14mer was next ligated to upstream 26mer and downstream 19mer RNA oligonucleotides by splinted ligation using T4 RNA ligase 2 and a single 44 nucleotide DNA splint with complementarity extending 15 nucleotides on either side of both ligation junctions (Table S1). The resulting ligated 59mer was in turn joined to a Cy5-labeled oligonucleotide by splinted ligation using T4 RNA ligase 2 and a 40 nucleotide DNA splint with 20 nucleotides complementarity on each side of the ligation junction to generate the full-length splicing substrate. The truncated form of the tandem 3' splice site substrate with a three nucleotide 3' exon was generated by cleavage of the full-length substrate with a 10-23 deoxyribozyme as previously described (Santoro and Joyce, 1997).

Expression and Purification of Recombinant Splicing Factors

A construct for expressing Prp2-K252A (bJPS2627) was generated by site-directed mutagenesis of *PRP2*-pRSETA (Krishnan et al., 2013), and the mutation was confirmed by sequencing. The plasmid bJPS2627 was transformed into Rosetta 2 (DE3) cells (EMD

Millipore). Cells were grown in Luria-Bertani broth at 37 °C until the OD_{600} reached 0.6 and then chilled on ice for 30 min. Expression of Prp2-K252A was induced with 0.6 mM isopropyl β-D-1-thiogalactopyranoside (IPTG) and 2% ethanol for 20 h at 18 °C. Cells were then harvested by centrifugation, suspended in lysis buffer (20 mM Tris-HCl [pH 8.0], 500 mM KCl, 10% glycerol), and lysed using a French press. The lysate was fractionated on a Ni^{2+}-nitrolotriacetic acid (Ni-NTA; Qiagen) column as described previously (Edwalds-Gilbert et al., 2000). The column fraction containing Prp2-K252A was then applied to a 3.4 mL 15-30% glycerol gradient (250 mM NaCl, 50 mM Tris-HCl [pH 8.0], 2 mM dithiothreitol [DTT], and 1 mM ethylenediaminetetraacetic acid [EDTA]) and spun at 47,000 rpm for 19h at 4 °C in an SW50.1 rotor. Gradient fractions were analyzed by SDS-polyacrylamide gel electrophoresis (PAGE) and fractions containing the Prp2-K252A peak were aliquoted, frozen in liquid N_2, and stored at -80 °C. Recombinant Prp16, Slu7, Prp18, Prp22, and Prp43 were expressed and purified as described previously (Ansari and Schwer, 1995; He et al., 2010; Koodathingal et al., 2010; Mayas et al., 2006; Zhang and Schwer, 1997).

In Vitro Splicing and Isolation and Chase of Stalled Spliceosomal Intermediates

Preparation of yeast splicing extracts (Mayas et al., 2006), depletion of Prp16 and Prp22 (Schwer, 2008), depletion and reconstitution of U6 (Fica et al., 2013), and in vitro splicing (Mayas et al., 2006) were performed essentially as described. To assemble stalled spliceosomal intermediates, 0.4 nM ^{32}P-labeled or 4 nM fluorescently-labeled substrate was incubated with 40% (v/v) yeast whole-cell extract in 250-500 μL reaction volumes at 20 °C for 30 min under standard splicing conditions (3% [w/v] PEG_{8000}, 60 mM potassium phosphate [pH 7.0], 0.5 mM free $MgCl_2$, and 2 mM ATP/$MgCl_2$; Mayas et al., 2006). Spliceosomes stalled in the assembled but inactive conformation, at the U4 release stage, were assembled in the presence of 0.5 mM

free $MgCl_2$ and 0.1 mM ATP/$MgCl_2$ (Tarn et al., 1993). To stall spliceosomes in the pre-catalytic conformation, the branching conformation, and the exon ligation conformation, splicing reactions were supplemented with ~150 nM Prp2-K252A, ~150 nM Prp16-K379A, and ~350 nM Prp22-K512A (Koodathingal et al., 2010; Mayas et al., 2006; this work), respectively, and the extract concentration was reduced to 32% (v/v) to accommodate the volume of added protein. The splicing reactions were then applied to 11 mL 15-40% glycerol gradients in G150 buffer (20 mM HEPES [pH 7.9], 150 mM KCl, 1.5 mM $MgCl_2$; Bessonov et al., 2008) and spun at 170,000 x g (37,000 rpm) for 13 h at 4 °C in a SW41 rotor. To prevent branching during spliceosome isolation, U6 U80-PS(S_P)-stalled spliceosomes were fractionated on glycerol gradients lacking $MgCl_2$ and containing 0.5 mM EDTA, in addition to 20 mM HEPES (pH 7.9), 50 mM NaCl. The activity of fractionated spliceosomes was generally insensitive to the concentration of $MgCl_2$ present during glycerol gradient fractionation. Fractions were collected from the tops of gradients, inspected by denaturing PAGE, frozen in liquid N_2, and stored at -80 °C. Fractions were selected for analysis by TIRF microscopy on the basis of enrichment for the desired substrate species (e.g. lariat intermediate and 5' exon in the case of spliceosomes stalled by Prp16-depletion or Prp16-K379A and mRNA in the case of spliceosomes stalled by Prp22-K512A). Glycerol gradient fractions containing stalled spliceosomes were thawed on ice, and then 10-30 μL of a gradient fraction was adjusted to a final volume of 100 μL in 0.5 mM $MgCl_2$, 60 mM potassium phosphate (pH 7.0), 3% (w/v) PEG_{8000}. Prp16-depleted spliceosomes were chased for 20 min at room temperature in reactions containing 10-30% (v/v) of a gradient fraction, 2.5 mM $MgCl_2$, 60 mM potassium phosphate (pH 7.0), 3% (w/v) PEG_{8000}, 2 mM ATP, 0.4 U/ μL rRNasIn (Promega), and ~150 nM Prp16, ~120 nM Slu7, ~120 nM Prp18, ~100 nM Prp22, and ~500 nM Prp43 as indicated. U6 U80-PS(S_P) spliceosomes were chased for 20 min at room temperature in reactions containing 1.25 mM $MgCl_2$, 60 mM potassium phosphate (pH 7.0), 3% (w/v) PEG_{8000}, and 2 mM ATP/$MgCl_2$ and 0.16 mM $CdCl_2$, as indicated. Aliquots of chase reactions were then either quenched with stop buffer containing 1 mM EDTA, 0.1% (w/v)

SDS and 50 mM sodium acetate (pH 5.2) and inspected by denaturing PAGE or immobilized for TIRF microscopy. Pre-mRNA present in Prp16-depleted spliceosomes assembled on d-brA substrate was site-specifically cleaved by incubating glycerol gradient fraction containing stalled spliceosomes (20% [v/v]) under standard splicing conditions in the presence of 0.2 U/μL RNaseH (Thermo Scientific) and 10 μM DNA oligonucleotide, as indicated, for 20 min at room temperature. Spliceosomes containing cleaved substrate were then chased through branching upon addition of ~150 nM Prp16 and incubation for 20 min at room temperature. Pre-mRNA present in U6 U80-PS(S_P)-stalled spliceosomes assembled on BS-labeled substrate was site-specifically cleaved by incubating glycerol gradient fraction containing stalled spliceosomes (15% [v/v]) under standard splicing conditions in the presence of 0.2 U/μL RNaseH (Thermo Scientific) and 10 μM DNA oligonucleotide, as indicated, for 20 min at room temperature. Spliceosomes containing cleaved substrate were then chased through branching upon addition of 0.25 mM $MgCl_2$, 0.25 mM $MnCl_2$, or 0.16 mM $CdCl_2$, as indicated, and incubation for 20 min at room temperature. Branching efficiency was calculated as (intron + lariat intermediate)/(intron + lariat intermediate + pre-mRNA). Exon ligation efficiency was calculated as mRNA/[mRNA + 5' exon]. As indicated by outlined boxes, panels in Figure 1B, 2A, 3A, 3E, 4B, 4C, 6A, S1B, S2C, S2F, S3A, S3C, S4B, S4C, S4E, S5C, and S6 were cropped and merged for clarity.

Preparation of Flow Cells and Immobilization of Spliceosomal Intermediates for TIRF Microscopy

Quartz slides and coverslips were PEG passivated with a 10:1 mixture of *O*-methyl-PEG and biotin-PEG and assembled into flow cells as described (Abelson et al., 2010). Then, 0.2 mg/mL streptavidin in 50 mM Tris-HCl (pH 7.5), 50 mM NaCl was flowed in and incubated for 20 min at

room temperature to allow streptavidin to bind biotin-PEG present on the surface of the slides. The flow cells were washed with 50 mM Tris-HCl (pH 7.5), 50 mM NaCl. The flow cells were blocked for 10 min at room temperature with 1 mg/mL BSA in 50 mM Tris-HCl (pH 7.5), 50 mM NaCl and then washed with 60 mM potassium phosphate (pH 7), 3% (w/v) PEG_{8000}. Stalled or chased spliceosomes were applied to flow cells in 100 μL volumes and incubated for 20 min at room temperature to allow spliceosomes to bind streptavidin via biotinylated Prp19 or Prp8. Flow cells were then washed (0.5 mM $MgCl_2$, 60 mM potassium phosphate [pH 7.0], 3% [w/v] PEG_{8000}) to remove unbound material. Spliceosomes were imaged in buffer containing 0.5 mM $MgCl_2$, 60 mM potassium phosphate (pH 7.0), 3% (w/v) PEG_{8000}, trolox (to suppress fluorophore blinking) and an oxygen scavenging system composed of protocatechuate and protocatechuate dioxygenase (to suppress photobleaching; Blanco and Walter, 2010). To ensure the specificity of spliceosome immobilization, each experiment included a control slide in which streptavidin was omitted. Omission of streptavidin reduced the number of immobilized spliceosomes by at least 20-fold.

Collection of smFRET Trajectories and Analysis

Data were collected using a prism-based TIRF microscope as described (Abelson et al., 2010; Krishnan et al., 2013). FRET was observed by direct excitation of the Cy3 donor fluorophore with a 532 nm laser over a period of 1-3 min and emission from both the donor and acceptor were recorded with 100 ms resolution with an intensified CCD camera. To confirm the presence of the acceptor fluorophore, Cy5 was directly excited using a 635 nm laser during the last ~60 s of the observation window. The duration of excitation was sufficient to observe photobleaching for the majority of molecules and thereby to confirm the presence of a single donor and single acceptor within in each spliceosome. Baseline correction of the raw donor and acceptor

emission data was performed using a morphological top-hat filter implemented in the IDL programming environment. Individual donor and acceptor trajectories were filtered by visual inspection (Blanco and Walter, 2010). FRET was calculated as $I_A/(I_A+I_D)$, where I_A and I_D are the fluorescence intensities of the acceptor and donor, respectively. Histograms describing the distribution of observed FRET values for a given population of spliceosomes were constructed by sampling the first 10 frames of data (1 s total) for each spliceosome. Although the substrate fluorophores are stable in the presence of splicing buffer alone, the assembly of spliceosomes on the substrate induces rapid fluorophore photobleaching (frequently within 5 s after initiating excitation), and consequently the 1 s sampling window was standardized to maximize the number spliceosomes analyzed and also to minimize any bias that may arise from enhanced photobleaching of subpopulations of spliceosome conformations. Histograms were fit with Gaussian distributions to reveal the underlying FRET states using Microcal Origin's Peak Analyzer routine. To determine approximate Gaussian centers for the underlying FRET states, a global fitting procedure was performed using all FRET values sampled to construct histograms under the conditions varied for a given experiment (e.g., all FRET values sampled for Figure 5, B to D). These center values were then used as initial guesses to fit individual histograms describing the FRET distribution for each condition within an experiment (e.g., Figure 5B). All reported changes in FRET distribution were observed in at least two independent spliceosome preparations.

Hidden Markov Model and Transition Occupancy Density Plot Analysis

Each single molecule trajectory was fit with a Hidden Markov Model (HMM) utilizing the publicly available vbFRET software package. Up to six states were allowed for fitting trajectories with the final number for each trajectory determined by vbFRET (generally, trajectories were fit by one to

three FRET states). To facilitate the comparison and quantification of states across molecules and conditions each state was reassigned to one of six evenly spaced FRET states determined by a modified k-means clustering approach utilizing built-in Matlab functions as previously described (Krishnan et al., 2013). Uncorrelated changes in either donor or acceptor fluorescence that lead to false FRET transitions were detected utilizing a regional anti-correlation filter. The regional anti-correlation filter scored each transition based on the cross-correlation of the donor and acceptor trajectories at the position of the putative transition using Matlab's cross-correlation function. Transition occupancy density plots (TODPs; ref. Blanco and Walter, 2010) were created based on the six FRET states and on the transitions that satisfied the cross-correlation filter. Peak heights revealed off of the diagonal reflect the fraction of molecules that contain a given HMM transition at least once. Molecules that occupied only one state, and thus did not transition, are revealed on the diagonal at the position of the occupied FRET state. All scripts for analysis are available upon request. Note that the six FRET states incorporated into the TODPs (in contrast to the two FRET states used to fit histograms) maximized our ability to detect transitions between similar FRET states. Consequently, one peak reflected in a histogram may be represented by two or more peaks in the TODPs. Further, the fraction of static molecules reported in Table S2 represents a lower bound as many transitions between adjacent FRET states likely arise as a consequence of experimental noise. The fraction of molecules that exhibit a given transition as indicated by the TODPs also represents a lower bound, because a given transition may be distributed over adjacent FRET states.

Bootstrap Analysis of FRET Probability Distributions

To assign statistical significance to the differences in FRET probability distributions for a pair of histograms, the mean and standard deviation for the frequencies of high and low FRET states was estimated using a bootstrap approach similar to the BOBA FRET analysis package (König et al., 2013). Briefly, for experimental conditions fit to two Gaussians a randomly selected subsample equivalent to 90% of the data was created 100 times. For each subsample a FRET probability distribution was created and fit with two Gaussians. The areas under the Gaussians (high or low FRET) for each subsample were measured and used to calculate means and standard deviations. The means and standard deviations of the measured areas were then utilized to measure significance using a two sample t-test utilizing the Matlab function ttest2.

Mapping the Branch Sites of Lariat Intermediates Formed by the br-dA Substrate

To generate a sequencing ladder, 250 fmol ^{32}P-labeled DNA primer (Integrated DNA Technologies; Table S1) was annealed to 80 fmol transcribed *UBC4* pre-mRNA and extended using Superscript II reverse transcriptase (Life Technologies) according to the manufacturer's instructions except that reactions contained 0.25 mM ddNTPs. To map branch sites, 250 fmol 5'-^{32}P-labeled DNA primer was annealed to ~2 fmol lariat intermediates and extended using AMV reverse transcriptase (Promega) according to the manufacturer's instructions.

UV Crosslinking

Splicing substrates site specifically modified with 4-thio-uracil and ^{32}P radiolabel were incubated with mock-, Prp16-, or Prp22-depleted extracts supplemented with recombinant protein as

indicated under standard in vitro splicing conditions (Mayas et al., 2006). Splicing reactions were then spotted onto parafilm covering an ice cold aluminum block and irradiated with an 8W, 365 nm UV lamp (Fisher Biotech FBUVLS-80) for 10 min at a distance of ~5 cm. 10 μL of the irradiated splicing reaction was then added to a 6 μL RNase T1 digest buffer (13 μM Tris-HCl [pH 7.4], 20 mM EDTA, 2.7x Complete protease inhibitor cocktail (Roche), 100 U/μL RNase T1 (Thermo Scientific) and incubated at 37 °C for 30 min. The reactions were then inspected by SDS-PAGE.

mRNA Release Assays

In vitro splicing of DNA substituted substrates was performed using yeast extract that was unsupplemented, supplemented with buffer, or supplemented with ~100 nM Prp22-K512A in volumes of 50 to 300 μL as described (Mayas et al., 2006). Splicing reactions were incubated at 20 °C for 60 min and the reactions were then fractionated on 15-40% glycerol gradients in G150 buffer (20 mM HEPES [pH 7.9], 150 mM KCl, 1.5 mM $MgCl_2$; Bessonov et al., 2008) and spun at 170,000 x g (37,000 rpm) for 13 h at 4 °C in a SW41 rotor. Fractions were collected from the tops of gradients, and inspected by denaturing PAGE.

Analysis of the Spliceosomal Footprint with XRN-1

A 100 μL splicing reaction supplemented with ~350 nM rPrp22-K512A and containing 0.4 nM 35|25 splicing substrate (Table S1) was incubated for 60 min at 20 °C and then fractionated on a 15-40% glycerol gradient as described above. Fractions containing spliceosomes stalled on mRNA were pooled and incubated at room temperature in 1x NEB buffer 3 (100 mM NaCl, 50 mM Tris-HCl [pH 7.9], 10 mM $MgCl_2$, 1 mM DTT) in the presence of 0.1 U/mL XRN-1 (NEB).

The digested mRNA was inspected by denaturing PAGE. The size of the protected mRNA fragment was determined by interpolation using RNA standards.

Supplemental References

Ansari, A., and Schwer, B. (1995). SLU7 and a novel activity, SSF1, act during the PRP16-dependent step of yeast pre-mRNA splicing. EMBO J. *14*, 4001-4009.

Bessonov, S., Anokhina, M., Will, C.L., Urlaub, H., and Lührmann, R. (2008). Isolation of an active step I spliceosome and composition of its RNP core. Nature *452*, 846-850.

Edwalds-Gilbert, G., Kim, D.H., Kim, S.H., Tseng, Y.H., Yu, Y., and Lin, R.-J. (2000). Dominant negative mutants of the yeast splicing factor Prp2 map to a putative cleft region in the helicase domain of DExD/H-box proteins. RNA *6*, 1106-1119.

Frederiksen, J.K., and Piccirilli, J.A. (2009). Separation of RNA phosphorothioate oligonucleotides by HPLC. Methods Enzymol. *468*, 289-309.

He, Y., Andersen, G.R., and Nielsen, K.H. (2010). Structural basis for the function of DEAH helicases. EMBO Rep. *11*, 180-186.

Hotz, H.R., and Schwer, B. (1998). Mutational analysis of the yeast DEAH-box splicing factor Prp16. Genetics *149*, 807-815.

König, S.L.B., Hadzic, M., Fiorini, E., Börner, R., Kowerko, D., Blackenhorn, W.U., and Sigel, R.K.O. (2013). BOBA FRET: Bootstrap-Based Analysis of Single-Molecule FRET Data. PLoS One *8*, e84157.

Liu, H.L., and Cheng, S.C. (2012). The interaction of Prp2 with a defined region of the intron is required for the first splicing reaction. Mol. Cell. Biol. *32*, 5056-5066.

Santoro, S.W., and Joyce, G.F. (1997). A general purpose RNA-cleaving DNA enzyme. Proc. Natl. Acad. Sci. U.S.A. *94*, 4262-4266.

Schwer, B., and Gross, C.H. (1998). Prp22, a DExH-box RNA helicase, plays two distinct roles in yeast pre-mRNA splicing. EMBO J. *17*, 2086-2094.

Tagwerker, C., Zhang, H., Wang, X., Larsen, L.S., Lathrop, R.H., Hatfield, G.W., Auer, B., Huang, L., and Kaiser, P. (2006). HB tag modules for PCR-based gene tagging and tandem affinity purification in Saccharomyces cerevisiae. Yeast *23*, 623-632.

Tseng, C.-K., and Cheng, S.-C. (2008). Both catalytic steps of nuclear pre-mRNA splicing are reversible. Science *320*, 1782-1784.

Yean, S.L., Wuenschell, G., Termini, J., and Lin, R.-J. (2000). Metal-ion coordination by U6 small nuclear RNA contributes to catalysis in the spliceosome. Nature *408*, 881-884.

Zhang, X., and Schwer, B. (1997). Functional and physical interaction between the yeast splicing factors Slu7 and Prp18. Nucleic Acids Res. *25*, 2146-2152.